1-6-2020

Granulins Modulate Liquid-Liquid Phase Separation and Aggregation of Prion-Like C-Terminal Domain of the Neurodegeneration-Associated Protein TDP-43

Anukool A. Bhopatkar
University of Southern Mississippi

Vladimir N. Uversky
University of South Florida

Vijay Rangachari
University of Southern Mississippi, Vijay.Rangachari@usm.edu

JBC Papers in Press. Published on January 6, 2020 as Manuscript RA119.011501
The latest version is at http://www.jbc.org/cgi/doi/10.1074/jbc.RA119.011501

Granulins modulate liquid-liquid phase separation and aggregation of prion-like C-terminal domain of the neurodegeneration-associated protein TDP-43

Anukool A. Bhopatkar*, Vladimir N. Uversky[#,§] and Vijayaraghavan Rangachari*[†].

*Department of Chemistry and Biochemistry, School of Mathematics and Natural Sciences, University of Southern Mississippi, Hattiesburg, MS 39406; [#]Department of Molecular Medicine and Byrd Alzheimer's Research Institute, Morsani College of Medicine, University of South Florida, Tampa, FL, 33620, USA; and [§]Laboratory of New Methods in Biology, Institute for Biological Instrumentation, Russian Academy of Sciences, 142290 Pushchino, Moscow Region, Russia

Running title: Interactions between TDP-43 C-terminal domain and GRNs

[†] Corresponding author: Vijay Rangachari, 118 College Drive #5043, University of Southern Mississippi, Hattiesburg, MS 39406. Tel: 601-266-6044; email: vijay.rangachari@um.edu

Keywords: Granulins, Progranulin, TDP-43, Liquid-liquid phase separation, Amyotrophic lateral sclerosis, Frontotemporal lobar degeneration, TAR DNA binding protein (TARDBP), Lou Gehrig's disease, intrinsically disordered protein, neurodegeneration

ABSTRACT

Tar DNA binding protein 43 (TDP-43) has emerged as a key player in many neurodegenerative pathologies including frontotemporal lobar degeneration (FTLD) and amyotrophic lateral sclerosis (ALS). Hallmarks of both FTLD and ALS are the toxic cytoplasmic inclusions of the prion-like C-terminal fragments of TDP-43 (TDP-43 CTD), formed upon proteolytic cleavage of full-length TDP-43 in the nucleus and subsequent transport to the cytoplasm. Both full-length TDP-43 and its CTD are also known to form stress granules (SGs) by coacervating with RNA in the cytoplasm during stress and may be involved in these pathologies. Furthermore, mutations in *PGRN* gene, leading to haploinsufficiency and diminished function of progranulin (PGRN) protein, are strongly linked to FTLD and ALS. Recent reports have indicated that proteolytic processing of PGRN to smaller protein modules called granulins (GRNs) contributes to FTLD and ALS progression, with specific GRNs exacerbating TDP-43–induced cytotoxicity. Here, we investigated the interactions between the proteolytic products of both TDP-43 and PGRN. Based on structural disorder and charge distributions, we hypothesized that GRNs -3 and -5 could interact with TDP-43 CTD. We also show that in both reducing and oxidizing conditions GRNs -3 and -5 interact with and differentially modulate TDP-43 CTD aggregation and/or liquid-liquid phase separation (LLPS) *in vitro*. While GRN-3 promoted insoluble aggregates of TDP-43 CTD, GRN-5 mediated LLPS. These results constitute the first observation of an interaction between GRNs and TDP-43, suggesting a mechanism by which attenuated PGRN function could lead to familial FTLD or ALS.

INTRODUCTION

Frontotemporal lobar degeneration (FTLD) is a neurodegenerative disorder characterized by progressive changes in behavior, speech, and personality among elderly patients (1,2). These changes are bought upon by a gradual atrophy of the frontal and anterior temporal lobes of the brain (3-6). Based on histopathology, heritable FTLD can be classified into the following subtypes: FTLD-TDP form, which is characterized by the presence of cytoplasmic inclusions of TAR DNA binding protein-43 (TDP-43), and which constitutes about half of all cases of FTLD (7); FTLD-Tau in which cytoplasmic inclusions of hyperphosphorylated tau are observed, and FTLD-FUS, which is associated with inclusions of an RNA-binding protein called fused in sarcoma (FUS) (8-12). The FTLD-TDP pathology is further sub-classified based on genetic and clinical presentation (13). Autosomal dominant mutations to progranulin gene (*PGRN*) are associated with type A while the hexanucleotide repeat expansions in *C9orf72* are present in type B cases (13). Inclusions of TDP-43 are also observed in patients with ALS (14-16). In addition to mutations in *TDP-43*, those in several genes have been linked to ALS including *FUS*, superoxide dismutase 1 (*SOD1*) and hexanucleotide repeat expansions in *C9orf72*. Since TDP-43-based neuropathology is present in ~50% of FTLD and ~97% of ALS cases (17), the protein represents a molecular link connecting these neurodegenerative diseases as a clinicopathological spectrum of the proteinopathies (15,18-20). It has also come to light that TDP-43 may contribute to the pathogenesis of Alzheimer disease (AD) via both β-amyloid (Aβ) dependent and independent pathways (21). Furthermore, TDP-43 abnormalities have also been associated with traumatic brain injury (chronic traumatic encephalopathy) in both pre-clinical and clinical studies (7), and observed in cognitively impaired persons in advanced age with hippocampal sclerosis, Huntington's disease and some other maladies (22). Due to the widespread prevalence of TDP-43 in neurodegenerative pathogenesis, all abnormalities involving the protein are classified into the category of 'TDP-43 proteinopathies' (22,23).

TDP-43 is a member of the heterogenous ribonucleoprotein family involved in transcriptional regulation and mRNA splicing in neurons (24). The protein consists of an N-terminal domain, two RNA recognition motifs (RRMs) followed by a low-complexity, glycine-rich C-terminal domain (25). The protein is known to dimerize through the N-terminal domain, while specific phosphomimic mutants within this domain disrupt its aggregation, liquid-liquid phase separation (LLPS) and RNA splicing activity (26,27). Although mainly localized in the nucleus, in the diseased state, a fraction of the full-length TDP-43 is proteolytically cleaved and thus generated 25 and 35 kDa (C25 and C35) C-terminal fragments are transported into the cytoplasm. These fragments form toxic insoluble inclusions observed

in ALS and FTLD-TDP patients (19,28,29). Under stress, both full-length and TDP-43 C-terminal fragments are also known to bind RNA and translocate to the cytosol, where they undergo LLPS to form the membraneless organelles called stress granules (29). LLPS has been increasingly observed in many cellular systems and are thought to be important in modulating many cellular functions (30-39). The precise mechanism of stress granule dynamics in TDP-43 pathophysiology remains unclear but many proteins are known to interact with, and partition into the phase separated droplets of TDP-43 (40,41). In FTLD and ALS, the aberrant LLPS of TDP-43 has emerged as a driving factor for the aggregation of the protein (40,42,43).

Progranulin (PGRN) is a 63.5 kDa secreted protein expressed in many cells including the neurons and in microglia (44-46), with pleiotropic roles in both physiological and pathological processes (47-51). The protein consists of seven and a half cysteine-rich modules called granulins (GRNs) (**Fig 1a**) (47,49,52-54), which are generated by proteolytic processing of PGRN by many proteases. PGRN and GRNs are observed to co-exist *in vivo* with opposing inflammatory functions (55). In FTLD, the observed inclusions of TDP-43 C-terminal fragments occur in the genetic backdrop of autosomal dominant, heterozygous mutations of *PGRN* that leads to haploinsuffiency of the PGRN protein. Homozygous *PGRN* mutations on the other hand lead to neuronal ceroid lipofuscinosis (NCL), a lysosomal storage disease (56). The production of GRNs in haploinsufficient, but not the null state in FTLD, suggests that they are key players in the disease phenotypes. This also indicates that the extenuation of PGRN function could arise from its increased proteolytic processing to generate GRNs (55). Indeed, GRNs are shown to interact with TDP-43 and exacerbate latter's levels and toxicity in *C.elegans*, establishing that PGRN cleavage to GRNs could represent an important part of the disease process in FTLD (57). Despite the growing evidence on the involvement of GRNs, their precise mechanisms in FTLD and related pathologies remain unclear. In this report, we sought to understand the interactions between GRNs and TDP-43 CTD, both of which are proteolytic products of their precursors, under reducing and oxidizing conditions *in vitro*. Our premise for investigations under reducing and oxidizing conditions stems from our previous observation that GRN-3 is active in both reduced and oxidized forms (58,59). Furthermore, GRNs' presence in both extra- and intracellular space led us to hypothesize that they may play a role under redox fluctuations. Here, we specifically investigated whether GRNs -3 and -5 are able to modulate LLPS or formation of insoluble inclusions of TDP-43 CTD, which shed insights into the potential role of GRNs in FTLD and ALS pathologies.

RESULTS

Structural disorder and charge distribution among GRNs and TDP-43 CTD suggest potential interactions. The 14.5 kDa construct of TDP-43 that constitutes residues 267-414 in the C-terminal domain (TDP-43 CTD) is a major part of the C25 proteolysis fragment that forms aberrant inclusions within the cytosol in FTLD and ALS patients (**Fig 1a**)(16). **Fig 1b** shows that TDP-43 CTD is largely disordered, and previous study indicated that this protein contains sequence of low-complexity that is involved in LLPS (60). On the other hand, GRNs (1-7) are small ~ 6 kDa proteins with the conserved sequence; $X_{2\text{-}3}CX_{5\text{-}6}CX_5CCX_8CCX_6$ $CCXDXXHCCPX_4CX_{5\text{-}6}CX$ (**Fig 1a**). The 12 conserved cysteine residues form six putative intramolecular disulfide bonds (61) (**Fig 1a**). **Fig 1c** and **Fig 1d** show that despite the fact that these proteins contain high levels of cysteine, which is the strongest order-promoting residue, GRN-3 and GRN-5 are predicted to be characterized by high levels of disorder. This is in line with the results of our previous studies, where we have shown that under reducing conditions, GRN-3 is fully disordered while in the oxidizing conditions, the protein obtains thermal stability via disulfide bonds without significant gain in the overall structure (59,62).

As a first step in understanding the effect of GRNs on TDP-43, here we report the interactions of GRNs 3 and 5 with TDP-43 CTD in both reducing and oxidizing conditions. GRN-5 was expressed and purified using the established method for GRN-3 (59) with some minor modifications (see Experimental Procedures). As observed previously with GRN-3 (59,62), we observed that GRN-5 too, in both reducing and oxidizing conditions, show a random coil disordered structure (Supplementary information; **Fig S1**). Intrinsic disorder predisposition of TDP-

43 and four other proteins (superoxide dismutase 1 (SOD1), FUS, a cofilin-binding protein C9orf72, and polypeptides generated as a result of its intronic hexanucleotide expansions, and actin-binding profilin-1 (PFN1)), which are considered as the major drivers of ALS and FTLD pathogenesis, recently revealed significant levels of disorder among these proteins (63,64). Here, we set out to determine whether disorder and charge distribution among TDP-43 CTD, and GRNs indicate interaction propensities. The primary sequence of GRN-5 is enriched in negatively charged residues and lack positively charged residues with a net pI of 4.01. On the other hand, TDP-43 CTD has an appreciable number of positively charged amino acids with a net pI of 9.52 (**Fig 1a**). The computed disorder predispositions show high degree of disorder for entire sequence of TDP-43 CTD (values > 0.5; **Fig 1b**), while GRN-3 and GRN-5 show disordered regions in both N- and C-terminal regions (**Fig 1c and 1d**). The linear net charge per residue (NCPR) plots for these proteins generated by CIDER computational platform (65) show that positively charged residues are preferentially concentrated within the 50 N-terminal residues of TDP-43 CTD (**Fig 1e**), whereas negatively charged residues are distributed over the entire sequence of GRN-5 (**Fig 1g**). Importantly, ANCHOR analysis (66,67) of the TDP-43 CTD construct utilized in this study revealed the existence of several disorder-based binding regions (residues 1-40, 66-99, 115-123, and 135-145). These regions represent molecular recognition features (MoRFs), which are intrinsically disordered segments that undergo folding on interaction with specific binding partners. Based on the counter-ionic character of the two proteins, we hypothesize that GRN-5 could interact with TDP-43 CTD and mediate LLPS. In addition, GRN-3 was chosen to test our hypothesis as this protein is also intrinsically disordered and has a pI of 5.33, but it contains both positive and negatively charged residues (**Fig 1a** and **Fig 1f**).

We also checked the amino acid sequence-based predispositions of TDP-43 CTD, GRN-3, and GRN-5 to undergo LLPS. To this end, the CatGRANULE algorithm was utilized that predicts LLPS propensity based on the analysis of the phase separation features linked to its primary sequence composition, structural disorder, and nucleic acid binding propensities (68). This analysis indicated that the CatGRANULE scores for TDP-43 CTD, GRN-3, and GRN-5 were 3.88, -3.06, and -2.83, respectively, indicating that only TDP-43 CTD has an intrinsic propensity for granule formation associated to liquid demixing under the physiological conditions. It has to be borne in mind that the positive CatGRANULE score for TDP-43CTD can be attributed to the fact that the algorithm was trained on the TDP-43 sequence. However, the negative CatGRANULE scores for GRNs are independent and decoupled to the use of TDP-43 sequence for the algorithm training.

GRN-5 but not GRN-3 initiates LLPS of TDP-43 CTD. To see whether GRNs mediate TDP-43 CTD phase separation, the two proteins were co-incubated in 2:1 molar ratio respectively, and the samples were monitored for turbidity increase and droplet formation by differential interference contrast (DIC) microscopy in both oxidizing (GRN-3 or GRN-5) and reducing (rGRN-3 or rGRN-5) conditions (**Fig 2**). At room temperature, 20 μM TDP-43 CTD buffered in 20 mM MES at pH 6.0 without salt in presence of 40 μM of GRN-5 or rGRN-5 formed a turbid solution instantly, similar to the known phase separation shown by TDP-43 CTD-RNA mixture (**Fig 2a**). On the other hand, incubation of TDP-43 CTD by itself or with 40 μM of GRN-3 or rGRN-3 did not show turbidity (**Fig 2a**). To define the phase boundaries of LLPS by TDP-43 CTD by under increasing GRN concentrations, 20 μM TDP-43 CTD was incubated with GRN-3, rGRN-3, GRN-5 and rGRN-5 in the absence of salt (**Fig 2b**). Both GRN-5 and rGRN-5 induce LLPS at concentrations as low 10 μM while neither GRN-3 nor rGRN-3 failed to induce any LLPS even at high concentrations (**Fig 2b)**. Next, phase boundaries of TDP-43 CTD LLPS as a function of GRN concentration and ionic strength were determined (**Fig 2c-g**). TDP-43 CTD control in the absence of GRNs but with increasing NaCl concentrations showed no LLPS below the physiological concentration of 150 mM salt (**Fig 2c**). GRN-3 showed LLPS above 100 mM NaCl over a large GRN concentration range (**Fig 2d**). rGRN-3 showed LLPS under relatively a narrow range of salt concentrations above 300 mM (**Fig 2e**). Both GRN-5 and rGRN-5 induced LLPS over a broad range of GRN and salt concentrations (**Fig 2f-g**). Only low GRN concentration and low ionic strength failed to induce LLPS of TDP-43 CTD. To visualize LLPS, the samples were observed

under a DIC microscope for 2:1 co-incubations of GRN:TDP-43 CTD in the same buffer conditions as mentioned above. The TDP-43 CTD control along with the mixture containing GRN-3 or rGRN-3 did not show the formation of liquid droplets for up to 6 hours (**Fig 2h**). In contrast, liquid droplets were observed almost instantaneously when TDP-43 CTD was co-incubated with rGRN-5, GRN-5 or RNA (**Fig 2h**). The droplets that were numerous and small initially, grew in size by coalescing with one another in the next six hours of incubation, displaying fluid-like characteristics. Together, the data suggest GRN-5 or rGRN-5, and not GRN-3 or rGRN-3, is able to initiate/enhance the phase separation of TDP-43 CTD significantly at low salt concentrations.

GRNs -3 and -5 differently modulate the LLPS and formation of ThT-positive aggregates of TDP-43 CTD. In FTLD and ALS pathologies, TDP-43 CTD is known to form toxic inclusions in the cytosol. Yet, ambiguity remains regarding the nature of these inclusions, with the presence of both thioflavin-T (ThT)-positive and ThT-negative aggregates has been reported (69-72). To see how GRNs affected the formation of TDP-43 CTD inclusions, we monitored ThT fluorescence for TDP-43 CTD samples in the presence of increasing concentrations of GRN-3, rGRN-3, GRN-5, or rGRN-5 at 37 °C (**Fig 3**). The sample of 20 μM TDP-43 CTD alone in 20 mM MES buffer at pH 6.0 showed a typical sigmoidal increase in fluorescence with a lag time of ~ 8 hours (●; **Fig 3**) indicating the formation of ThT-positive species. For GRN-3 incubations, increasing its stoichiometry from 0.1 to 4-fold excess to that of TDP-43 CTD showed increasing lag time of aggregation (**Fig 3a**). The 0.1-fold incubation showed the smallest lag time with 12 hours, while the 4-fold excess GRN-3 showed the highest lag time of ~22 hours. Similarly, under fully reducing conditions, 0.1 to 4-fold excess of rGRN-3 also inhibited TDP-43 CTD aggregation, but to a much lesser degree than GRN-3, with lag times ranging between 8 and 15 hours (**Fig 3b**). Similarly, incubation of GRN-5 in increasing concentrations (0.1 to 4-fold excess) with TDP-43 CTD showed an overall inhibition of the TDP-43 CTD fibrillation by increasing the lag times (12 to 36 hours, respectively) (**Fig 3c**). Incubations of rGRN-5 with TDP-43 CTD, on the other hand, showed no discernable lag time but an instantaneous linear increase in ThT fluorescence for all stoichiometric incubations **(Fig 3a**; inset). These data suggest that GRN-3 and GRN-5 interact with TDP-43 CTD differently to modulate latter's aggregation. Furthermore, the observed instantaneous LLPS of TDP-43 CTD in the presence of GRN-5 and rGRN-5 (**Fig 2**) raises the possibility of the ThT dye partitioning into the droplets formed, resulting in the higher ThT fluorescence observed. To investigate this, the reactions were visualized by fluorescence microscopy using another amyloid binding dye called thioflavin-S (ThS). Both ThT and ThS are known to detect amyloid aggregates (73,74). A 10 μM buffered solution of ThS was added to the samples containing 20 μM TDP-43 CTD alone (**Fig 3i**) and in the presence of 40 μM GRNs; GRN-3 (**Fig 3e**), rGRN-3 (**Fig 3f**), GRN-5 (**Fig 3g**), and rGRN-5 (**Fig 3h**). Instantaneously upon addition, TDP-43 CTD alone and with either GRN-3 or rGRN-3 showed no aggregate formation, and a disperse blue fluorescent haze was observed (**Fig 3i , Fig 3e** and **Fig 3f**; 0h). It has to be noted that the use of a 420-480 nm band pass emission filter generates a blue color to ThS. The same reactions after 36 hours showed more concentrated areas where ThS was observed that coincided with the presence of inclusions (**Fig 3i**, **Fig 3e** and **Fig 3f**; 36h). GRN-5 or rGRN-5 on the other hand, showed the presence of ThS within the droplets even at 0 hours (**Fig 3g** and **Fig 3h**; 0h), which continued to be present even after 36 hours (**Fig 3g** and **Fig 3h**; 36h). These data suggest that, *a*) ThS (or ThT) could partition into the droplets, *b*) enhanced fluorescent signals could emerge due to partitioning into the droplets, and *c*) a small amount of ThT-positive species could be present within the droplets.

Both GRNs colocalize with TDP-43 CTD within the droplets or aggregates. To probe whether the droplets are complex coacervates of TDP-43 CTD and GRNs or formed without GRNs' partitioning into the separated phase, fluorescence microscopy was used to observe the colocalization of the two proteins. TDP-43 CTD and GRNs, labeled with HiLyte 647 and HiLyte 405, respectively, were incubated separately under oxidizing and reducing condition and monitored for 36 hours (**Fig 4**). As expected, TDP-43 CTD by itself did not form phase separated droplets immediately after incubation (**Fig 4a**; 0h), and over the next 36 hours, sparse deposits of aggregated

protein were observed (**Fig 4a**; 18h and 36h). Co-incubations of GRN-3 or rGRN-3 with TDP-43 CTD showed no LLPS immediately after incubation (**Fig 4b** and **Fig 4c**; 0h), parallel to the observation by DIC and turbidity (**Fig 2**). Even after 36 hours, no phase separated liquid droplets, but insoluble, fibrillar deposits were observed (**Fig 4b** and **Fig 4c**; 18h and 36h) that bind amyloid dyes as shown above (**Fig 3**). Moreover, the GRNs were observed to be localized in the vicinity of TDP-43 CTD deposits as well as within them (**Fig 4b** and **Fig 4c**; 36h). On the other hand, co-incubations of both GRN-5 and rGRN-5 with TDP-43 CTD resulted in the emergence of well-defined liquid droplets immediately after incubation (**Fig 4d** and **Fig 4e**; 0h). The number of droplets increased during the next 36 hours of incubation, with some becoming more distorted spherical droplets (**Fig 4d** and **Fig 4e**; 18h and 36h). Importantly, both GRNs (blue) colocalize within the droplets formed by TDP-43 CTD (red). To further glean into the physical nature of the droplets or insoluble inclusions formed, fluorescence recovery after photobleaching (FRAP) was conducted (**Fig 4f-j**). After 36h of incubation, TDP-43 CTD control showed no recovery after bleaching indicative of insoluble solid nature of the aggregates (**Fig 4f**). A similar behavior was observed with the coincubations of TDP-43 CTD with GRN-3 or rGRN-3 (**Fig 4g** and **4h**) suggesting that GRN-3 in both reducing and oxidized states promoted insoluble fibrils of TDP-43 CTD as seen from the microscopy images. However, GRN-5 in both redox states (GRN-5 and rGRN-5) showed exponential fluorescence recovery immediately after incubation indicating fluid property of the droplet (**Fig 4i** and **4j**; 0h). After 36h, the extent of recovery was slightly mitigated indicating a possible "gelation" of the droplet (**Fig 4i** and **4j**; 36h). Together, the data further confirm that both GRN-5 and rGRN-5 induce LLPS with TDP-43 CTD by coacervation. On the other hand, GRN-3 does not induce LLPS but forms insoluble deposits of aggregated forms of TDP-43 CTD, indicating the differential specificity for the two GRNs in interacting with TDP-43 CTD. In other words, both GRNs could initiate different biophysical processes; while the presence of GRN-3 or rGRN-3 lead to insoluble aggregates, those of GRN-5 or rGRN-5 result in the droplet formation that could change to gelation or aggregates over time.

To further confirm and quantify the partitioning and co-localization of TDP-43 CTD and GRNs, the relative amounts of the proteins within the droplets as well as the deposits were quantified by MALDI-TOF mass spectrometry. Using a known amount of insulin (6.45 ng/μL) as an external standard, the mass spectra were obtained (**Figs 5a-e**) and the relative quantities of the proteins were calculated and normalized (detailed in Materials and Methods). Aliquots of the samples used in **Fig 3** and **Fig 4** were obtained after 36 hours for quantitative analysis. Both GRN-3 and rGRN-3 showed positive correlation between the amount of GRN co-incubated and TDP-43 CTD with the amount of GRN-3 or rGRN-3 increasing in the sedimented pellet with increase in GRN:TDP-43 CTD molar ratios (**Fig 5f** and **Fig 5g**). More importantly, the ratio of GRN to TDP-43 CTD intensities remained below one, suggesting GRN-3 or rGRN-3 may augment TDP-43 CTD aggregation by nucleating and not by forming a co-complex in stochiometric proportions. This observation is similar to the recently observed ability of GRN-3 and rGRN-3 to form fibrils of amyloid-β(1-42) (Aβ42) peptide involved in Alzheimer disease (AD), where minimal GRN was observed in the pellet (58). On the other hand, the ratio of GRN-to-TDP-43 CTD obtained from the sedimented droplets of TDP-43 CTD and GRN-5 or rGRN-5 co-incubations did not show a linear increase with increasing concentrations of GRN as observed with GRN-3 (**Fig 5h** and **Fig 5i**). For co-incubations of GRN-5 and rGRN-5, the GRN-to-TDP-43 CTD ratio remained at 0.75 and 1.1, respectively, over the entire range of molar ratios. It is known that the phenomenon of coacervation is dependent on a defined valency of interactions among the molecules which remain fixed within the dense phase (75-78). One could speculate that the network of weak interactions necessary to stabilize the TDP-43 CTD droplets could be achieved by accommodating equimolar proportions of GRN-5 or rGRN-5 within the droplets.

GRNs modulate liquid droplets formed by TDP-43 CTD and RNA. One of the main aspects of TDP-43 pathobiology is the coacervation with RNA molecules to form membraneless organelles in the form of stress granules (79-81). To see whether GRNs 3 and 5 are able to interact with, and modulate liquid droplets (LDs) of TDP-43 CTD and RNA, torula yeast RNA extract was co-

incubated with TDP-43 CTD in the presence or absence of GRNs. As expected, control LDs containing a mixture of 20 μM TDP-43 CTD and 40 μg/mL RNA showed high turbidity (**Fig 6a**). Solutions containing a mixture of LDs and 40 μM of GRN-5 showed an increase in turbidity as compared to LD control (**Fig 6a**). The sample containing 40 μM rGRN-5 and LDs did not show appreciable change in turbidity. Similarly, solutions containing a mixture of LDs and GRN-3 or rGRN-3 showed a slight decrease or no change turbidity levels as compared to the control (**Fig 6a**). In order to see how GRNs affect the formation of ThT-positive inclusions of the LDs, the reactions were monitored by ThT fluorescence (**Fig 6b-c**). As expected, the co-incubation of RNA with TDP-43 CTD did not show any ThT increase as they form LDs (**Fig 6b** and **Fig 6c**) as compared to the TDP-43 CTD alone (●; **Fig 6b** and **Fig 6c**). Inclusion of rGRN-3 to the RNA and TDP-43 CTD mixture significantly increased the rate of ThT-positive aggregates of TDP-43 CTD (**Fig 6b**) but slightly delayed the aggregation compared to TDP-43 CTD alone or with rGRN-3 (**Fig 6b**). Similar augmentation of aggregation was observed with the co-incubation of GRN-3 and TDP-43 CTD-RNA mixture (**Fig 6b**) although the increase in rate of aggregation was less pronounced with GRN-3 as compared to rGRN-3 as previously observed in **Fig 3**. Co-incubation of rGRN-5 to the TDP-43 CTD-RNA mixture 'rescued' the aggregation of TDP-43 CTD with a linear increase in ThT fluorescence observed within hours of incubation (**Fig 6c**). However, augmentation of ThT-positive aggregates was also pronounced with the co-incubation of GRN-5 (**Fig 6c**). These data indicate that GRNs are able to modify LD to promote aggregates of TDP-43 CTD.

To further understand the mechanism of GRNs' influence on LD, co-incubations of fluorescently-tagged samples were monitored by DIC microscopy. As expected, TDP-43 CTD-RNA showed LD formation immediately after incubation that remained for 36 hours (**Fig 6d**). Co-incubation of GRN-3 or GRN-3 with the mixture of TDP-43 CTD and RNA showed neither a marked change to the droplet shape or size nor the GRN colocalized within the droplet (**Fig 6e-f**). After 36 hours, a marginal increase in LD size was observed with GRN colocalized within the droplets (**Fig 6e-f**). However, the samples showed distortions in the morphology of LDs accompanied by an overall reduction in the size during the course of the experiment (**Fig 6e-f**). Addition of GRN-5 to TDP-43 CTD-RNA mixture also showed the formation of droplets immediately with GRN colocalized within the droplets, which fused and grew bigger in size during the next 36 hours, with both TDP-43 CTD and GRN-5 colocalizing within the LDs (**Fig 6g**). Addition of rGRN-5 to TDP-43 CTD-RNA mixture led to droplet formation which grew in number but not in size during the same time (**Fig 6h**). rGRN-5 also co-localized with TDP-43 CTD within the LDs.

To probe the internal dynamics of the LD droplets, FRAP was monitored temporally on labelled TDP-43 CTD in presence of RNA and GRNs. The fluorescence recovery rates for the control LDs formed by TDP-43 CTD and RNA showed near identical rates at both 0 and 36 hours, indicating preservation of internal mobility and dynamism over the incubation period (**Fig 6i**). LDs formed in the presence of either GRN-3 or rGRN-3 showed a marked level of decrease in the internal mobility of the droplets during the 36 hours of incubation (**Fig j-k**). Similarly, LDs formed in presence of both redox forms of GRN-5 displayed a decreased fluorescence recovery after 36 hours indicating an inhibition of internal mobility, which could indicate the maturation of the droplets into gels, process commonly known as 'gelation' (**Fig 6l**; GRN5 and **Fig 6m**; rGRN-5). Similar to the observation of GRN-5 and TDP-43 CTD where 'gelated' droplets eventually transition to solid aggregates (Fig S2), it is possible that these 'gelated' LD also eventually form insoluble aggregates of TDP-43 CTD. The increase in ThT fluorescence (**Fig 6c**) can be explained by the fact that ThS (and likely ThT) is able to partitions into the droplets and fluoresces as observed (**Fig 3**). The results obtained suggest that both GRNs 3 and 5 in redox conditions co-localize and stabilize the LDs formed by TDP-43 CTD and RNA. What cellular ramifications this may have on stress response by stress granules is remains to be seen.

DISCUSSION

Link between PGRN and familial FTLD/ALS is well-established with the implication of autosomal dominant mutations in *PGRN*, which leads to the protein's haploinsuffiency. The loss of

PGRN function in these pathologies is also speculated to arise at a posttranscriptional level with increased PGRN proteolysis (82). GRN immunopositivities have indeed been observed in a region-specific manner in both AD and FTLD human brains (83). Furthermore, the production of GRNs in haploinsufficient and not null state in familial FTLD suggests that they may be key players in the disease phenotypes. Support for this thought comes from the observation that GRNs interact with TDP-43 and exacerbate latter's levels and toxicity in *C.elegans* (57). Moreover, the recent discovery of PGRN/GRNs being associated with lysosomal dysfunction (84) also posits the question whether GRNs could be involved in autophagic fate of TDP-43 inclusions under redox stress. The results presented here attempts to answer some of the key questions regarding GRNs and TDP-43 CTD such as how GRNs modulate the dynamics between LD and fibril formation of TDP-43 CTD and do LDs facilitate the formation of insoluble TDP-43 CTD inclusions.

The findings of this study showcase how GRNs -3 and -5 modulate the dynamics of TDP-43 CTD in forming insoluble aggregates or LDs in both oxidizing and reducing conditions. It is clear from the data that GRN-3 and GRN-5 affect TDP-43 CTD aggregation via disparate mechanisms; while GRN-3 induces the formation of insoluble inclusions, GRN-5 coacervates with TDP-43 CTD to undergo LLPS in both reduced and oxidized forms, an interaction which is likely to be driven by the counter-ionic electrostatic characteristics of TDP-43 CTD and the negatively charged GRN-5 (85-87). Furthermore, GRN-3 and GRN-5 also modify LDs formed by the coacervation of RNA and TDP-43 CTD. Specifically, GRN-3 in both redox states accelerate the formation of ThT-positive, insoluble aggregates of TDP-43 CTD. This observation supports the one by Salazar and co-workers who observed exacerbation of TDP-43 toxicity in *C.elegans* by GRN-3 and GRN-7 (57). GRN-5, on the other hand seems to remodify the LDs by inducing gelation within the 36-hour time period, which changes to fibril formation after extended time period (supplementary **Fig S2**). At this point, it is unclear as to what cellular ramifications do the gelation of LDs by GRN-5 have, but our on-going investigations will glean into this aspect in the future. Nevertheless, our results provide the first in vitro evidence for an interaction between GRN and TDP-43 CTD.

The increasing relevance of GRNs in FTLD and associated neurodegenerative disorders imparts significance to the results presented in this study. Despite its significance, how haploinsufficiency of PGRN results in TDP-43 inclusions in FTLD and ALS patients remains unknown. Common mutations associated with PGRN haploinsufficiency have been linked to mutant mRNA degradation (88) which several groups have identified leads directly to reduced circulating levels of PGRN (89-91). A few have also argued that increased proteolysis of PGRN as the reason for haploinsufficiency, which leads to increase in GRN levels (57). A more recent study established that more effective proteolytic processing of cathepsin D, an aspartyl protease that is known to cleave PGRN, occurs in the presence of GRNs (92), which seem to support the idea that generation of GRNs to be the reason for decreased availability of PGRN. Results presented in this study identify a potential mechanism by which GRNs interact with TDP-43 CTD and modulate the latter's ability to aggregate and/or phase separate (**Fig 6**). Based on our data we can hypothesize that the selective GRNs interact with free TDP-43 CTD to augment its aggregation and potentially its cytotoxicity. Alternatively, under redox stress, GRNs can interact with LDs to modulate the dynamics within the droplets towards the formation of insoluble inclusions or lead to a decreased stress response. These aspects, along with whether and how these processes are regulated by phosphorylation and other mutations within GRNs and TDP-43 are currently being investigated in our laboratory, and the results obtained will be reported at a later time.

EXPERIMENTAL PROCEDURES

Expression and purification of recombinant proteins

Granulins (GRN-3 & GRN-5): Unlabeled GRN-3 was expressed and purified from *E. coli* SHuffle^{TM} cells (New England Biolabs) as described previously (62), while unlabeled GRN-5 and ^{15}N labeled GRN-5 were expressed in Origami 2 DE3 (Invitrogen). Briefly, the proteins were expressed as a GRN:trxA fusion construct and purified using immobilized-nickel affinity chromatography. The fusion protein was then cleaved by addition of restriction grade thrombin

(Bovine, BioPharm Laboratories) at 1U per 1 mg of the protein to remove both trxA and the His-tag. The reaction was incubated at room temperature (~25°C) for 22-24 hours. The protein was then fractionated on a semi-preparative Jupiter® 5 µm 10x250 mm C18 reverse phase HPLC column (Phenomenex), using a gradient elution of 60 – 80 % acetonitrile containing 0.1% TFA as previously described (62). The concentration of the proteins was estimated spectrophotometrically using molar extinction coefficients of 6250 $M^{-1}cm^{-1}$ for GRN-3 and 7740 $M^{-1}cm^{-1}$ for GRN-5 at 280 nm. The number of free cysteines was calculated from Elman's assay and by iodoacetamide labeling as previously reported (62). rGRN-3 and rGRN-5 were generated by the addition of 2 mM Tris(2-carboxyethyl)phosphine hydrochloride (TCEP) to the HPLC fractionated protein for 2 hours at room temperature and were used as the reduced form. ^{15}N labeled GRN-3,5 were generated by growing the cells in M9 minimal media enriched with $^{15}NH_4Cl$.

TDP-43 CTD. The plasmid for the TDP-43 CTD expression was a gift from Dr. Nicolas Fawzi at Brown University (Addgene plasmid # 98669; http://n2t.net/addgene:98669; RRID:Addgene 98669). The protein was expressed as a fusion construct with a His-tag (His_6) at the N-Terminal followed by a TEV cleavage site The plasmid was expressed in *E.coli* BL21 Star™ (DE3) cells (Life Technologies). Transformed cells were grown at 37°C in LB medium supplemented with 100µg/ml of kanamycin. Overexpression of the protein was induced by adding isopropyl β-D-1-thiogalactopyranoside (IPTG) to a final concentration of 0.5 mM at an optical density ($O.D_{600}$) of 0.5-0.7 AU. After overnight induction at room temperature (~25°C), cells were harvested by centrifugation (15000xg, 4 °C) and used immediately or stored at −20°C. The cells were resuspended in lysis buffer (20 mM Tris pH 8.0, 500 mM NaCl, 5 mM imidazole, 6 M urea). 0.5 mM phenylmethylsulfonyl fluoride (PMSF) was also added to the resuspension. Cells were lysed using Misonix XL-2000. The lysate was centrifuged at 20000 xg, 4°C, for 1 hour to remove cellular debris. The supernatant was incubated with Ni-NTA resin at 4°C for 2 hours. The slurry was resuspended in Kimble Kontes Flex column and washed with wash buffers (20 mM Tris pH 8.0, 500 mM NaCl, 6 M Urea) of 15 mM and 30 mM imidazole and protein was eluted in elution buffer (20 mM Tris pH 8.0, 500 mM NaCl, 6 M Urea, 150 mM imidazole). Eluate was buffer exchanged into storage buffer (20 mM Tris pH 8.0, 500 mM NaCl, 2 M Urea) and concentrated using Amicon Ultra-Centrifugal units (Millipore). Concentrated protein was flash frozen and stored at -80°C. Concentrated aliquots were thawed on ice and desalted into 20 mM MES pH 6.0 using Zeba Desalting Spin Columns (Thermo) and used as such for studies.

Thioflavin-T fluorescence

The aggregation kinetics of TDP-43 CTD were monitored using Thioflavin-T (ThT) on a BioTek Synergy H1 microplate reader. 20 µM TDP-43 CTD under varying reaction conditions was incubated at 37°C for 36 hours in presence of 10 µM ThT. Samples were excited at 440 nm and emission was monitored at 480 nm. The ThT kinetic data was fit using the Boltzmann function on Origin 8.5.

MALDI-ToF mass spectrometry

Pellet and droplet characterization of the co-incubated protein complexes was performed on a Bruker Datonics Microflex LT/SH ToF-MS system. Samples from aggregation kinetic reactions were recovered after a period of 36 hours. The recovered samples were spun down at 18000 xg and supernatant was decanted. The pellet obtained was then resuspended in equal volume of reaction buffer (20 mM MES, pH 6.0). The pellet and supernatant fractions were then prepared for MALDI-MS by mixing with 6.5 ng of insulin (external standard). Additionally, the pellet samples were dissolved with formic acid in a 1:1 ratio to allow disaggregation of fibrils and other insoluble complexes. Both aliquots were then spotted onto a Bruker MSP 96 MicroScout Target with 1:1 ratio of sample:sinapinic acid matrix in saturated acetonitrile and water. Instrument calibration was performed using Bruker Protein Calibration Standard I (Bruker Daltonics).

Differential Interference Contrast (DIC)

The phase separation was monitored using DIC on a Leica DMIL LED microscope under 20x or 40x magnification with a DIC polarizing filter. The reactions were observed on a clear-bottom Nunc™ MicroWell™ 96-Well Microplates (Thermo).

Fluorescence microscopy

For colocalization studies of GRNs and TDP-43 CTD during the course of their interactions, labeling of the respective proteins with amine-reactive fluorescent dyes was performed and visualization was done on a Zeiss LSM 510 Meta confocal microscope at 40x or 63x magnification under oil-immersion with a DIC polarizing filter. Briefly, TDP-43 CTD was labelled with HiLyte-647 (AnaSpec) and GRN-3,5 were labelled with HiLyte-405 (AnaSpec). Free dyes were removed via the use of desalting columns; Zeba Desalting Spin Columns (Thermo) for labeled TDP-43 CTD and Clarion™ MINI Spin Columns, Desalt S-25 (SorbTech) for labeled GRN-3,5. 20 uM TDP-43 CTD was mixed with 40 µM GRN-3,5 or 40 ug/mL of RNA. A ratio of 1% Labeled: 99% Unlabeled proteins was used for both TDP-43 CTD and GRNs. Reactions were performed on the following experimental setup: A glass cover-slip was attached onto one end of a two-side open ended 96 well plate (Greiner Bio-One). Reactions were loaded into a well and covered with an optically clear plate-sealing film (Thermo). Reactions were then monitored at certain timepoints. Similarly, for observing the localization of ThS, 10 µM ThS (AAT bioquest) was added to sample containing 20 µM TDP-43 CTD with 40 µM of GRNs. Samples were visualized using the setup described above on a Zeiss LSM 510 Meta with 420-480 band pass emission filter

FRAP

FRAP assays were performed in open-ended 96 well plates as described above; 10 µM TDP-43 CTD was mixed with 20 µM GRN-3,5 or 20 µg/mL of RNA. Reactions were monitored 10 mins after mixing to allow deposition of suitable droplets onto the bottom of the well, which were used for bleaching. TDP-43 CTD labelled with HiLyte-647 (AnaSpec) was used as the probe in the assays. LSM 510 Meta confocal microscope at 63x magnification under oil-immersion with a DIC polarizing filter and FRAP module. The region of interest was bleached with 633 nm laser line with 100% bleaching intensity for 750 iterations and imaging was performed at 5% laser intensity for 120 secs after bleaching. Numerical aperture was kept at 0.69 AU.

NMR spectroscopy

The HMQC NMR spectra for 20 µM ^{15}N GRN-5 or rGRN-5 resuspended in 20 mM MES (pH 6.0) with 10% D_2O was acquired on a Bruker Advance – III-HD 850 MHz NMR spectrometer equipped with a Bruker TCI cryoprobe at the high field NMR facility of University of Alabama, Birmingham as described previously(62).

Computational analysis of TDP-43 CTD, GRN-3, and GRN-5

Per-residue intrinsic disorder predispositions of TDP-43 CTD, GRN-3, and GRN-5 were evaluated by a set of commonly used disorder predictors, such as PONDR® VLXT(93) , PONDR® VSL2 (94) , and PONDR® VL3 (95) available on the PONDR site (http://www.pondr.com) PONDR® FIT (96) accessible at the DisProt site (http://original.disprot.org/metapredictor.php), and the IUPred computational platform available at IUPred2A site (https://iupred2a.elte.hu/) that allows identification either short or long regions of intrinsic disorder, IUPred-L and IUPred-S (97-100). For each query protein, the outputs of these individual predictors were used to calculate a consensus disorder profile by averaging disorder profiles of individual predictors. The outputs of these tools are represented as real numbers between 1 (ideal prediction of disorder) and 0 (ideal prediction of order). A threshold of ≥0.5 was used to identify disordered residues and regions in query proteins. A protein region was considered flexible, if its disorder propensity was in a range from 0.2 to 0.5. Results of this multiparametric computational analysis are presented in a form of mean disorder propensity calculated by averaging disorder profiles of individual predictors. Use of consensus for evaluation of intrinsic disorder is motivated by empirical observations that this approach usually increases the predictive performance compared to the use of a single predictor (96,101-108). CIDER computational platform (65) was used to generate linear net charge per residue diagrams for query proteins, whereas the sequence-based propensities of TDP-43 CTD, GRN-3, and GRN-5 for granule formation associated to liquid demixing under the physiological conditions were evaluated by CatGRANULE algorithm (68) , which generates positive and negative scores for proteins capable and not capable of granule formation, respectively. Finally, the presence of disorder-based binding

sites in TDP-43 CTD was evaluated by the ANCHOR algorithm (66,67).

ACKNOWLEDGEMENTS

The authors would like to thank the following agencies for financial support: National Institute of Aging (1R56AG062292-01 to VR and RF1AG055088 to VNU), National Institute of General Medical Sciences (R01GM120634 to VR), and the National Science Foundation (NSF CBET 1802793 to VR). The authors also thank the National Center for Research Resources (5P20RR01647-11) and the National Institute of General Medical Sciences (8 P20 GM103476-11) from the National Institutes of Health for funding through INBRE for the use of their core facilities. The authors thank Dr. Nicholas Fawzi at Brown University for his advice on TDP-43 CTD purification. The authors also thank Dr. Jonathan Lindner at USM for his help in the use of fluorescence microscopy.

CONFILCT OF INTERST STATEMENT

The authors declare that they have no conflicts of interest with the contents of this article.

REFERENCES

1. Neary, D., Snowden, J. S., Gustafson, L., Passant, U., Stuss, D., Black, S., Freedman, M., Kertesz, A., Robert, P. H., Albert, M., Boone, K., Miller, B. L., Cummings, J., and Benson, D. F. (1998) Frontotemporal lobar degeneration: a consensus on clinical diagnostic criteria. *Neurology* **51**, 1546-1554
2. Robert, P. H., Lafont, V., Snowden, J. S., and Lebert, F. (1999) [Diagnostic criteria for fronto-temporal lobe degeneration]. *L'Encephale* **25**, 612-621
3. Fukui, T., and Kertesz, A. (2000) Volumetric study of lobar atrophy in Pick complex and Alzheimer's disease. *Journal of the neurological sciences* **174**, 111-121
4. Hulette, C. M., and Crain, B. J. (1992) Lobar atrophy without Pick bodies. *Clinical neuropathology* **11**, 151-156
5. Cooper, P. N., Siddons, C. A., and Mann, D. M. (1996) Patterns of glial cell activity in fronto-temporal dementia (lobar atrophy). *Neuropathology and applied neurobiology* **22**, 17-22
6. Bocti, C., Rockel, C., Roy, P., Gao, F., and Black, S. E. (2006) Topographical patterns of lobar atrophy in frontotemporal dementia and Alzheimer's disease. *Dementia and geriatric cognitive disorders* **21**, 364-372
7. Heyburn, L., Sajja, V., and Long, J. B. (2019) The Role of TDP-43 in Military-Relevant TBI and Chronic Neurodegeneration. *Frontiers in neurology* **10**, 680
8. Bang, J., Spina, S., and Miller, B. L. (2015) Frontotemporal dementia. *Lancet* **386**, 1672-1682
9. Prasad, A., Bharathi, V., Sivalingam, V., Girdhar, A., and Patel, B. K. (2019) Molecular Mechanisms of TDP-43 Misfolding and Pathology in Amyotrophic Lateral Sclerosis. *Frontiers in molecular neuroscience* **12**, 25
10. Berning, B. A., and Walker, A. K. (2019) The Pathobiology of TDP-43 C-Terminal Fragments in ALS and FTLD. *Frontiers in neuroscience* **13**, 335
11. Sun, Y., and Chakrabartty, A. (2017) Phase to Phase with TDP-43. *Biochemistry* **56**, 809-823
12. Irwin, D. J., Cairns, N. J., Grossman, M., McMillan, C. T., Lee, E. B., Van Deerlin, V. M., Lee, V. M. Y., and Trojanowski, J. Q. (2015) Frontotemporal lobar degeneration: defining phenotypic diversity through personalized medicine. *Acta Neuropathologica* **129**, 469-491
13. Mackenzie, I. R., Neumann, M., Baborie, A., Sampathu, D. M., Du Plessis, D., Jaros, E., Perry, R. H., Trojanowski, J. Q., Mann, D. M., and Lee, V. M. (2011) A harmonized classification system for FTLD-TDP pathology. *Acta Neuropathol* **122**, 111-113
14. Hasegawa, M., Arai, T., Nonaka, T., Kametani, F., Yoshida, M., Hashizume, Y., Beach, T. G., Buratti, E., Baralle, F., Morita, M., Nakano, I., Oda, T., Tsuchiya, K., and Akiyama, H. (2008) Phosphorylated TDP-43 in frontotemporal lobar degeneration and amyotrophic lateral sclerosis. *Annals of neurology* **64**, 60-70
15. Arai, T., Hasegawa, M., Akiyama, H., Ikeda, K., Nonaka, T., Mori, H., Mann, D., Tsuchiya, K., Yoshida, M., Hashizume, Y., and Oda, T. (2006) TDP-43 is a component of ubiquitin-positive tau-negative inclusions in frontotemporal lobar degeneration and amyotrophic lateral sclerosis. *Biochemical and biophysical research communications* **351**, 602-611
16. Igaz, L. M., Kwong, L. K., Xu, Y., Truax, A. C., Uryu, K., Neumann, M., Clark, C. M., Elman, L. B., Miller, B. L., Grossman, M., McCluskey, L. F., Trojanowski, J. Q., and Lee, V. M. (2008) Enrichment of C-terminal fragments in TAR DNA-binding protein-43 cytoplasmic inclusions in brain but not in spinal cord of frontotemporal lobar degeneration and amyotrophic lateral sclerosis. *The American journal of pathology* **173**, 182-194
17. Ling, S. C., Polymenidou, M., and Cleveland, D. W. (2013) Converging mechanisms in ALS and FTD: disrupted RNA and protein homeostasis. *Neuron* **79**, 416-438

18. Cascella, R., Fani, G., Bigi, A., Chiti, F., and Cecchi, C. (2019) Partial Failure of Proteostasis Systems Counteracting TDP-43 Aggregates in Neurodegenerative Diseases. *International journal of molecular sciences* **20**
19. Neumann, M., Sampathu, D. M., Kwong, L. K., Truax, A. C., Micsenyi, M. C., Chou, T. T., Bruce, J., Schuck, T., Grossman, M., Clark, C. M., McCluskey, L. F., Miller, B. L., Masliah, E., Mackenzie, I. R., Feldman, H., Feiden, W., Kretzschmar, H. A., Trojanowski, J. Q., and Lee, V. M. (2006) Ubiquitinated TDP-43 in frontotemporal lobar degeneration and amyotrophic lateral sclerosis. *Science (New York, N.Y.)* **314**, 130-133
20. Davidson, Y., Kelley, T., Mackenzie, I. R., Pickering-Brown, S., Du Plessis, D., Neary, D., Snowden, J. S., and Mann, D. M. (2007) Ubiquitinated pathological lesions in frontotemporal lobar degeneration contain the TAR DNA-binding protein, TDP-43. *Acta Neuropathol* **113**, 521-533
21. Chang, X. L., Tan, M. S., Tan, L., and Yu, J. T. (2016) The Role of TDP-43 in Alzheimer's Disease. *Molecular neurobiology* **53**, 3349-3359
22. Chornenkyy, Y., Fardo, D. W., and Nelson, P. T. (2019) Tau and TDP-43 proteinopathies: kindred pathologic cascades and genetic pleiotropy. *Laboratory investigation; a journal of technical methods and pathology* **99**, 993-1007
23. Guo, L., and Shorter, J. (2017) Biology and Pathobiology of TDP-43 and Emergent Therapeutic Strategies. *Cold Spring Harbor perspectives in medicine* **7**
24. Ayala, Y. M., Pantano, S., D'Ambrogio, A., Buratti, E., Brindisi, A., Marchetti, C., Romano, M., and Baralle, F. E. (2005) Human, Drosophila, and C.elegans TDP43: nucleic acid binding properties and splicing regulatory function. *Journal of molecular biology* **348**, 575-588
25. Ayala, Y. M., Zago, P., D'Ambrogio, A., Xu, Y. F., Petrucelli, L., Buratti, E., and Baralle, F. E. (2008) Structural determinants of the cellular localization and shuttling of TDP-43. *Journal of cell science* **121**, 3778-3785
26. Afroz, T., Hock, E.-M., Ernst, P., Foglieni, C., Jambeau, M., Gilhespy, L. A. B., Laferriere, F., Maniecka, Z., Plückthun, A., Mittl, P., Paganetti, P., Allain, F. H. T., and Polymenidou, M. (2017) Functional and dynamic polymerization of the ALS-linked protein TDP-43 antagonizes its pathologic aggregation. *Nature Communications* **8**, 45
27. Wang, A., Conicella, A. E., Schmidt, H. B., Martin, E. W., Rhoads, S. N., Reeb, A. N., Nourse, A., Ramirez Montero, D., Ryan, V. H., Rohatgi, R., Shewmaker, F., Naik, M. T., Mittag, T., Ayala, Y. M., and Fawzi, N. L. (2018) A single N-terminal phosphomimic disrupts TDP-43 polymerization, phase separation, and RNA splicing. *The EMBO Journal* **37**, e97452
28. Zhang, Y. J., Xu, Y. F., Cook, C., Gendron, T. F., Roettges, P., Link, C. D., Lin, W. L., Tong, J., Castanedes-Casey, M., Ash, P., Gass, J., Rangachari, V., Buratti, E., Baralle, F., Golde, T. E., Dickson, D. W., and Petrucelli, L. (2009) Aberrant cleavage of TDP-43 enhances aggregation and cellular toxicity. *Proceedings of the National Academy of Sciences of the United States of America* **106**, 7607-7612
29. Kitamura, A., Nakayama, Y., Shibasaki, A., Taki, A., Yuno, S., Takeda, K., Yahara, M., Tanabe, N., and Kinjo, M. (2016) Interaction of RNA with a C-terminal fragment of the amyotrophic lateral sclerosis-associated TDP43 reduces cytotoxicity. *Scientific reports* **6**, 19230
30. Hyman, A. A., Weber, C. A., and Jülicher, F. (2014) Liquid-Liquid Phase Separation in Biology. *Annual Review of Cell and Developmental Biology* **30**, 39-58
31. Bouchard, J. J., Otero, J. H., Scott, D. C., Szulc, E., Martin, E. W., Sabri, N., Granata, D., Marzahn, M. R., Lindorff-Larsen, K., Salvatella, X., Schulman, B. A., and Mittag, T. (2018) Cancer Mutations of the Tumor Suppressor SPOP Disrupt the Formation of Active, Phase-Separated Compartments. *Molecular Cell* **72**, 19-36.e18
32. Burke, Kathleen A., Janke, Abigail M., Rhine, Christy L., and Fawzi, Nicolas L. (2015) Residue-by-Residue View of In Vitro FUS Granules that Bind the C-Terminal Domain of RNA Polymerase II. *Molecular Cell* **60**, 231-241

33. Dao, T. P., Kolaitis, R.-M., Kim, H. J., O'Donovan, K., Martyniak, B., Colicino, E., Hehnly, H., Taylor, J. P., and Castañeda, C. A. (2018) Ubiquitin Modulates Liquid-Liquid Phase Separation of UBQLN2 via Disruption of Multivalent Interactions. *Molecular Cell* **69**, 965-978.e966
34. Das, R. K., Ruff, K. M., and Pappu, R. V. (2015) Relating sequence encoded information to form and function of intrinsically disordered proteins. *Current Opinion in Structural Biology* **32**, 102-112
35. Delarue, M., Brittingham, G. P., Pfeffer, S., Surovtsev, I. V., Pinglay, S., Kennedy, K. J., Schaffer, M., Gutierrez, J. I., Sang, D., Poterewicz, G., Chung, J. K., Plitzko, J. M., Groves, J. T., Jacobs-Wagner, C., Engel, B. D., and Holt, L. J. (2018) mTORC1 Controls Phase Separation and the Biophysical Properties of the Cytoplasm by Tuning Crowding. *Cell* **174**, 338-349.e320
36. Fei, J., Jadaliha, M., Harmon, T. S., Li, I. T. S., Hua, B., Hao, Q., Holehouse, A. S., Reyer, M., Sun, Q., Freier, S. M., Pappu, R. V., Prasanth, K. V., and Ha, T. (2017) Quantitative analysis of multilayer organization of proteins and RNA in nuclear speckles at super resolution. *Journal of cell science* **130**, 4180
37. Dine, E., Gil, A. A., Uribe, G., Brangwynne, C. P., and Toettcher, J. E. (2018) Protein Phase Separation Provides Long-Term Memory of Transient Spatial Stimuli. *Cell Systems* **6**, 655-663.e655
38. Kwon, I., Kato, M., Xiang, S., Wu, L., Theodoropoulos, P., Mirzaei, H., Han, T., Xie, S., Corden, Jeffry L., and McKnight, Steven L. (2013) Phosphorylation-Regulated Binding of RNA Polymerase II to Fibrous Polymers of Low-Complexity Domains. *Cell* **155**, 1049-1060
39. Kroschwald, S., Munder, M. C., Maharana, S., Franzmann, T. M., Richter, D., Ruer, M., Hyman, A. A., and Alberti, S. (2018) Different Material States of Pub1 Condensates Define Distinct Modes of Stress Adaptation and Recovery. *Cell Reports* **23**, 3327-3339
40. Gasset-Rosa, F., Lu, S., Yu, H., Chen, C., Melamed, Z., Guo, L., Shorter, J., Da Cruz, S., and Cleveland, D. W. (2019) Cytoplasmic TDP-43 De-mixing Independent of Stress Granules Drives Inhibition of Nuclear Import, Loss of Nuclear TDP-43, and Cell Death. *Neuron* **102**, 339-357.e337
41. McDonald, K. K., Aulas, A., Destroismaisons, L., Pickles, S., Beleac, E., Camu, W., Rouleau, G. A., and Vande Velde, C. (2011) TAR DNA-binding protein 43 (TDP-43) regulates stress granule dynamics via differential regulation of G3BP and TIA-1. *Human molecular genetics* **20**, 1400-1410
42. Mann, J. R., Gleixner, A. M., Mauna, J. C., Gomes, E., DeChellis-Marks, M. R., Needham, P. G., Copley, K. E., Hurtle, B., Portz, B., Pyles, N. J., Guo, L., Calder, C. B., Wills, Z. P., Pandey, U. B., Kofler, J. K., Brodsky, J. L., Thathiah, A., Shorter, J., and Donnelly, C. J. (2019) RNA Binding Antagonizes Neurotoxic Phase Transitions of TDP-43. *Neuron* **102**, 321-338.e328
43. Babinchak, W. M., Haider, R., Dumm, B. K., Sarkar, P., Surewicz, K., Choi, J.-K., and Surewicz, W. K. (2019) The role of liquid-liquid phase separation in aggregation of the TDP-43 low complexity domain. *Journal of Biological Chemistry*
44. Moisse, K., Volkening, K., Leystra-Lantz, C., Welch, I., Hill, T., and Strong, M. J. (2009) Divergent patterns of cytosolic TDP-43 and neuronal progranulin expression following axotomy: implications for TDP-43 in the physiological response to neuronal injury. *Brain research* **1249**, 202-211
45. Petkau, T. L., Neal, S., Orban, P., MacDonald, J., Hill, A., Lu, G., Feldman, H., Mackenzie, I., and Leavitt, B. (2010) Progranulin expression in the developing and adult murine brain. *Journal of Comparative Neurology* **518**, 3931-3947
46. Ryan, C. L., Baranowski, D. C., Chitramuthu, B. P., Malik, S., Li, Z., Cao, M., Minotti, S., Durham, H. D., Kay, D. G., and Shaw, C. A. (2009) Progranulin is expressed within motor neurons and promotes neuronal cell survival. *BMC neuroscience* **10**, 1
47. Baba, T., Hoff, H. B., Nemoto, H., Lee, H., Orth, J., Arai, Y., and Gerton, G. L. (1993) Acrogranin, an acrosomal cysteine-rich glycoprotein, is the precursor of the growth-modulating peptides, granulins, and epithelins, and is expressed in somatic as well as male germ cells. *Molecular reproduction and development* **34**, 233-243
48. Bateman, A., and Bennett, H. P. (1998) Granulins: the structure and function of an emerging family of growth factors. *The Journal of endocrinology* **158**, 145-151

49. Plowman, G. D., Green, J. M., Neubauer, M. G., Buckley, S. D., McDonald, V. L., Todaro, G. J., and Shoyab, M. (1992) The epithelin precursor encodes two proteins with opposing activities on epithelial cell growth. *Journal of Biological Chemistry* **267**, 13073-13078
50. Zanocco-Marani, T., Bateman, A., Romano, G., Valentinis, B., He, Z.-H., and Baserga, R. (1999) Biological activities and signaling pathways of the granulin/epithelin precursor. *Cancer Research* **59**, 5331-5340
51. Zhou, J., Gao, G., Crabb, J. W., and Serrero, G. (1993) Purification of an autocrine growth factor homologous with mouse epithelin precursor from a highly tumorigenic cell line. *Journal of Biological Chemistry* **268**, 10863-10869
52. Bateman, A., Belcourt, D., Bennett, H., Lazure, C., and Solomon, S. (1990) Granulins, a novel class of peptide from leukocytes. *Biochemical and biophysical research communications* **173**, 1161-1168
53. Bhandari, V., Palfree, R., and Bateman, A. (1992) Isolation and sequence of the granulin precursor cDNA from human bone marrow reveals tandem cysteine-rich granulin domains. *Proceedings of the National Academy of Sciences* **89**, 1715-1719
54. Shoyab, M., McDonald, V. L., Byles, C., Todaro, G. J., and Plowman, G. D. (1990) Epithelins 1 and 2: isolation and characterization of two cysteine-rich growth-modulating proteins. *Proceedings of the National Academy of Sciences* **87**, 7912-7916
55. Zhu, J., Nathan, C., Jin, W., Sim, D., Ashcroft, G. S., Wahl, S. M., Lacomis, L., Erdjument-Bromage, H., Tempst, P., Wright, C. D., and Ding, A. (2002) Conversion of proepithelin to epithelins: roles of SLPI and elastase in host defense and wound repair. *Cell* **111**, 867-878
56. Chitramuthu, B. P., Bennett, H. P. J., and Bateman, A. (2017) Progranulin: a new avenue towards the understanding and treatment of neurodegenerative disease. *Brain : a journal of neurology* **140**, 3081-3104
57. Salazar, D. A., Butler, V. J., Argouarch, A. R., Hsu, T. Y., Mason, A., Nakamura, A., McCurdy, H., Cox, D., Ng, R., Pan, G., Seeley, W. W., Miller, B. L., and Kao, A. W. (2015) The Progranulin Cleavage Products, Granulins, Exacerbate TDP-43 Toxicity and Increase TDP-43 Levels. *The Journal of neuroscience : the official journal of the Society for Neuroscience* **35**, 9315-9328
58. Bhopatkar, A. A., Ghag, G., Wolf, L. M., Dean, D. N., Moss, M. A., and Rangachari, V. (2019) Cysteine-rich granulin-3 rapidly promotes amyloid-beta fibrils in both redox states. *The Biochemical journal* **476**, 859-873
59. Ghag, G., Wolf, L. M., Reed, R. G., Van Der Munnik, N. P., Mundoma, C., Moss, M. A., and Rangachari, V. (2016) Fully reduced granulin-B is intrinsically disordered and displays concentration-dependent dynamics. *Protein engineering, design & selection : PEDS* **29**, 177-186
60. Conicella, A. E., Zerze, G. H., Mittal, J., and Fawzi, N. L. (2016) ALS Mutations Disrupt Phase Separation Mediated by alpha-Helical Structure in the TDP-43 Low-Complexity C-Terminal Domain. *Structure (London, England : 1993)* **24**, 1537-1549
61. Tolkatchev, D., Malik, S., Vinogradova, A., Wang, P., Chen, Z., Xu, P., Bennett, H. P., Bateman, A., and Ni, F. (2008) Structure dissection of human progranulin identifies well-folded granulin/epithelin modules with unique functional activities. *Protein science : a publication of the Protein Society* **17**, 711-724
62. Ghag, G., Holler, C. J., Taylor, G., Kukar, T. L., Uversky, V. N., and Rangachari, V. (2017) Disulfide bonds and disorder in granulin-3: An unusual handshake between structural stability and plasticity. *Protein science : a publication of the Protein Society* **26**, 1759-1772
63. Santamaria, N., Alhothali, M., Alfonso, M. H., Breydo, L., and Uversky, V. N. (2017) Intrinsic disorder in proteins involved in amyotrophic lateral sclerosis. *Cellular and molecular life sciences : CMLS* **74**, 1297-1318
64. Uversky, V. N. (2017) The roles of intrinsic disorder-based liquid-liquid phase transitions in the "Dr. Jekyll-Mr. Hyde" behavior of proteins involved in amyotrophic lateral sclerosis and frontotemporal lobar degeneration. *Autophagy* **13**, 2115-2162

65. Holehouse, A. S., Das, R. K., Ahad, J. N., Richardson, M. O., and Pappu, R. V. (2017) CIDER: Resources to Analyze Sequence-Ensemble Relationships of Intrinsically Disordered Proteins. *Biophysical journal* **112**, 16-21
66. Meszaros, B., Simon, I., and Dosztanyi, Z. (2009) Prediction of protein binding regions in disordered proteins. *PLoS computational biology* **5**, e1000376
67. Dosztanyi, Z., Meszaros, B., and Simon, I. (2009) ANCHOR: web server for predicting protein binding regions in disordered proteins. *Bioinformatics (Oxford, England)* **25**, 2745-2746
68. Bolognesi, B., Lorenzo Gotor, N., Dhar, R., Cirillo, D., Baldrighi, M., Tartaglia, G. G., and Lehner, B. (2016) A Concentration-Dependent Liquid Phase Separation Can Cause Toxicity upon Increased Protein Expression. *Cell Rep* **16**, 222-231
69. Furukawa, Y., Kaneko, K., Watanabe, S., Yamanaka, K., and Nukina, N. (2011) A seeding reaction recapitulates intracellular formation of Sarkosyl-insoluble transactivation response element (TAR) DNA-binding protein-43 inclusions. *The Journal of biological chemistry* **286**, 18664-18672
70. Jiang, L.-L., Che, M.-X., Zhao, J., Zhou, C.-J., Xie, M.-Y., Li, H.-Y., He, J.-H., and Hu, H.-Y. (2013) Structural transformation of the amyloidogenic core region of TDP-43 protein initiates its aggregation and cytoplasmic inclusion. *The Journal of biological chemistry* **288**, 19614-19624
71. Capitini, C., Conti, S., Perni, M., Guidi, F., Cascella, R., De Poli, A., Penco, A., Relini, A., Cecchi, C., and Chiti, F. (2014) TDP-43 inclusion bodies formed in bacteria are structurally amorphous, non-amyloid and inherently toxic to neuroblastoma cells. *PloS one* **9**, e86720
72. Johnson, B. S., Snead, D., Lee, J. J., McCaffery, J. M., Shorter, J., and Gitler, A. D. (2009) TDP-43 Is Intrinsically Aggregation-prone, and Amyotrophic Lateral Sclerosis-linked Mutations Accelerate Aggregation and Increase Toxicity. *Journal of Biological Chemistry* **284**, 20329-20339
73. Biancalana, M., and Koide, S. (2010) Molecular mechanism of Thioflavin-T binding to amyloid fibrils. *Biochim Biophys Acta* **1804**, 1405-1412
74. Elhaddaoui, A., Pigorsch, E., Delacourte, A., and Turrell, S. (1995) Competition of congo red and thioflavin S binding to amyloid sites in alzheimer's diseased tissue. *Biospectroscopy* **1**, 351-356
75. Rao, B. S., and Parker, R. (2017) Numerous interactions act redundantly to assemble a tunable size of P bodies in <em>Saccharomyces cerevisiae</em&gt. *Proceedings of the National Academy of Sciences* **114**, E9569
76. Banani, S. F., Rice, A. M., Peeples, W. B., Lin, Y., Jain, S., Parker, R., and Rosen, M. K. (2016) Compositional Control of Phase-Separated Cellular Bodies. *Cell* **166**, 651-663
77. Wang, J., Choi, J.-M., Holehouse, A. S., Lee, H. O., Zhang, X., Jahnel, M., Maharana, S., Lemaitre, R., Pozniakovsky, A., Drechsel, D., Poser, I., Pappu, R. V., Alberti, S., and Hyman, A. A. (2018) A Molecular Grammar Governing the Driving Forces for Phase Separation of Prion-like RNA Binding Proteins. *Cell* **174**, 688-699.e616
78. Prather, L. J., Weerasekare, G. M., Sima, M., Quinn, C., and Stewart, R. J. (2019) Aqueous Liquid-Liquid Phase Separation of Natural and Synthetic Polyguanidiniums. *Polymers* **11**
79. Tollervey, J. R., Curk, T., Rogelj, B., Briese, M., Cereda, M., Kayikci, M., Konig, J., Hortobagyi, T., Nishimura, A. L., Zupunski, V., Patani, R., Chandran, S., Rot, G., Zupan, B., Shaw, C. E., and Ule, J. (2011) Characterizing the RNA targets and position-dependent splicing regulation by TDP-43. *Nature neuroscience* **14**, 452-458
80. Khalfallah, Y., Kuta, R., Grasmuck, C., Prat, A., Durham, H. D., and Vande Velde, C. (2018) TDP-43 regulation of stress granule dynamics in neurodegenerative disease-relevant cell types. *Scientific reports* **8**, 7551
81. Chen, Y., and Cohen, T. J. (2019) Aggregation of the nucleic acid–binding protein TDP-43 occurs via distinct routes that are coordinated with stress granule formation. *Journal of Biological Chemistry*
82. Kleinberger, G., Capell, A., Haass, C., and Van Broeckhoven, C. (2013) Mechanisms of granulin deficiency: lessons from cellular and animal models. *Molecular neurobiology* **47**, 337-360
83. Mao, Q., Wang, D., Li, Y., Kohler, M., Wilson, J., Parton, Z., Shmaltsuyeva, B., Gursel, D., Rademakers, R., Weintraub, S., Mesulam, M. M., Xia, H., and Bigio, E. H. (2017) Disease and

Region Specificity of Granulin Immunopositivities in Alzheimer Disease and Frontotemporal Lobar Degeneration. *Journal of neuropathology and experimental neurology* **76**, 957-968
84. Holler, C. J., Taylor, G., Deng, Q., and Kukar, T. (2017) Intracellular Proteolysis of Progranulin Generates Stable, Lysosomal Granulins that Are Haploinsufficient in Patients with Frontotemporal Dementia Caused by GRN Mutations. *eNeuro* **4**
85. Mitrea, D. M., and Kriwacki, R. W. (2016) Phase separation in biology; functional organization of a higher order. *Cell Commun Signal* **14**, 1-1
86. Boyko, S., Qi, X., Chen, T.-H., Surewicz, K., and Surewicz, W. K. (2019) Liquid-liquid phase separation of tau protein: The crucial role of electrostatic interactions. *Journal of Biological Chemistry*
87. Pak, Chi W., Kosno, M., Holehouse, Alex S., Padrick, Shae B., Mittal, A., Ali, R., Yunus, Ali A., Liu, David R., Pappu, Rohit V., and Rosen, Michael K. (2016) Sequence Determinants of Intracellular Phase Separation by Complex Coacervation of a Disordered Protein. *Molecular Cell* **63**, 72-85
88. Coppola, G., Karydas, A., Rademakers, R., Wang, Q., Baker, M., Hutton, M., Miller, B. L., and Geschwind, D. H. (2008) Gene expression study on peripheral blood identifies progranulin mutations. *Annals of neurology* **64**, 92-96
89. Ghidoni, R., Benussi, L., Glionna, M., Franzoni, M., and Binetti, G. (2008) Low plasma progranulin levels predict progranulin mutations in frontotemporal lobar degeneration. *Neurology* **71**, 1235-1239
90. Finch, N., Baker, M., Crook, R., Swanson, K., Kuntz, K., Surtees, R., Bisceglio, G., Rovelet-Lecrux, A., Boeve, B., Petersen, R. C., Dickson, D. W., Younkin, S. G., Deramecourt, V., Crook, J., Graff-Radford, N. R., and Rademakers, R. (2009) Plasma progranulin levels predict progranulin mutation status in frontotemporal dementia patients and asymptomatic family members. *Brain : a journal of neurology* **132**, 583-591
91. Sleegers, K., Brouwers, N., Van Damme, P., Engelborghs, S., Gijselinck, I., van der Zee, J., Peeters, K., Mattheijssens, M., Cruts, M., Vandenberghe, R., De Deyn, P. P., Robberecht, W., and Van Broeckhoven, C. (2009) Serum biomarker for progranulin-associated frontotemporal lobar degeneration. *Annals of neurology* **65**, 603-609
92. Butler, V. J., Cortopassi, W. A., Gururaj, S., Wang, A. L., Pierce, O. M., Jacobson, M. P., and Kao, A. W. (2019) Multi-Granulin Domain Peptides Bind to Pro-Cathepsin D and Stimulate Its Enzymatic Activity More Effectively Than Progranulin in Vitro. *Biochemistry* **58**, 2670-2674
93. Romero, P., Obradovic, Z., Li, X., Garner, E. C., Brown, C. J., and Dunker, A. K. (2001) Sequence complexity of disordered protein. *Proteins* **42**, 38-48
94. Peng, K., Radivojac, P., Vucetic, S., Dunker, A. K., and Obradovic, Z. (2006) Length-dependent prediction of protein intrinsic disorder. *BMC bioinformatics* **7**, 208
95. Peng, K., Vucetic, S., Radivojac, P., Brown, C. J., Dunker, A. K., and Obradovic, Z. (2005) Optimizing long intrinsic disorder predictors with protein evolutionary information. *Journal of bioinformatics and computational biology* **3**, 35-60
96. Xue, B., Dunbrack, R. L., Williams, R. W., Dunker, A. K., and Uversky, V. N. (2010) PONDR-FIT: a meta-predictor of intrinsically disordered amino acids. *Biochim Biophys Acta* **1804**, 996-1010
97. Dosztanyi, Z., Csizmok, V., Tompa, P., and Simon, I. (2005) The pairwise energy content estimated from amino acid composition discriminates between folded and intrinsically unstructured proteins. *Journal of molecular biology* **347**, 827-839
98. Dosztanyi, Z., Csizmok, V., Tompa, P., and Simon, I. (2005) IUPred: web server for the prediction of intrinsically unstructured regions of proteins based on estimated energy content. *Bioinformatics (Oxford, England)* **21**, 3433-3434
99. Dosztanyi, Z. (2018) Prediction of protein disorder based on IUPred. *Protein science : a publication of the Protein Society* **27**, 331-340
100. Meszaros, B., Erdos, G., and Dosztanyi, Z. (2018) IUPred2A: context-dependent prediction of protein disorder as a function of redox state and protein binding. *Nucleic acids research* **46**, W329-w337

101. Ferron, F., Longhi, S., Canard, B., and Karlin, D. (2006) A practical overview of protein disorder prediction methods. *Proteins* **65**, 1-14
102. Lieutaud, P., Canard, B., and Longhi, S. (2008) MeDor: a metaserver for predicting protein disorder. *BMC genomics* **9 Suppl 2**, S25
103. He, B., Wang, K., Liu, Y., Xue, B., Uversky, V. N., and Dunker, A. K. (2009) Predicting intrinsic disorder in proteins: an overview. *Cell research* **19**, 929-949
104. Peng, Z., and Kurgan, L. (2012) On the complementarity of the consensus-based disorder prediction. *Pacific Symposium on Biocomputing. Pacific Symposium on Biocomputing*, 176-187
105. Fan, X., and Kurgan, L. (2014) Accurate prediction of disorder in protein chains with a comprehensive and empirically designed consensus. *Journal of biomolecular structure & dynamics* **32**, 448-464
106. Walsh, I., Giollo, M., Di Domenico, T., Ferrari, C., Zimmermann, O., and Tosatto, S. C. (2015) Comprehensive large-scale assessment of intrinsic protein disorder. *Bioinformatics (Oxford, England)* **31**, 201-208
107. Meng, F., Uversky, V., and Kurgan, L. (2017) Computational Prediction of Intrinsic Disorder in Proteins. *Current protocols in protein science* **88**, 2.16.11-12.16.14
108. Meng, F., Uversky, V. N., and Kurgan, L. (2017) Comprehensive review of methods for prediction of intrinsic disorder and its molecular functions. *Cellular and molecular life sciences : CMLS* **74**, 3069-3090

FIGURES

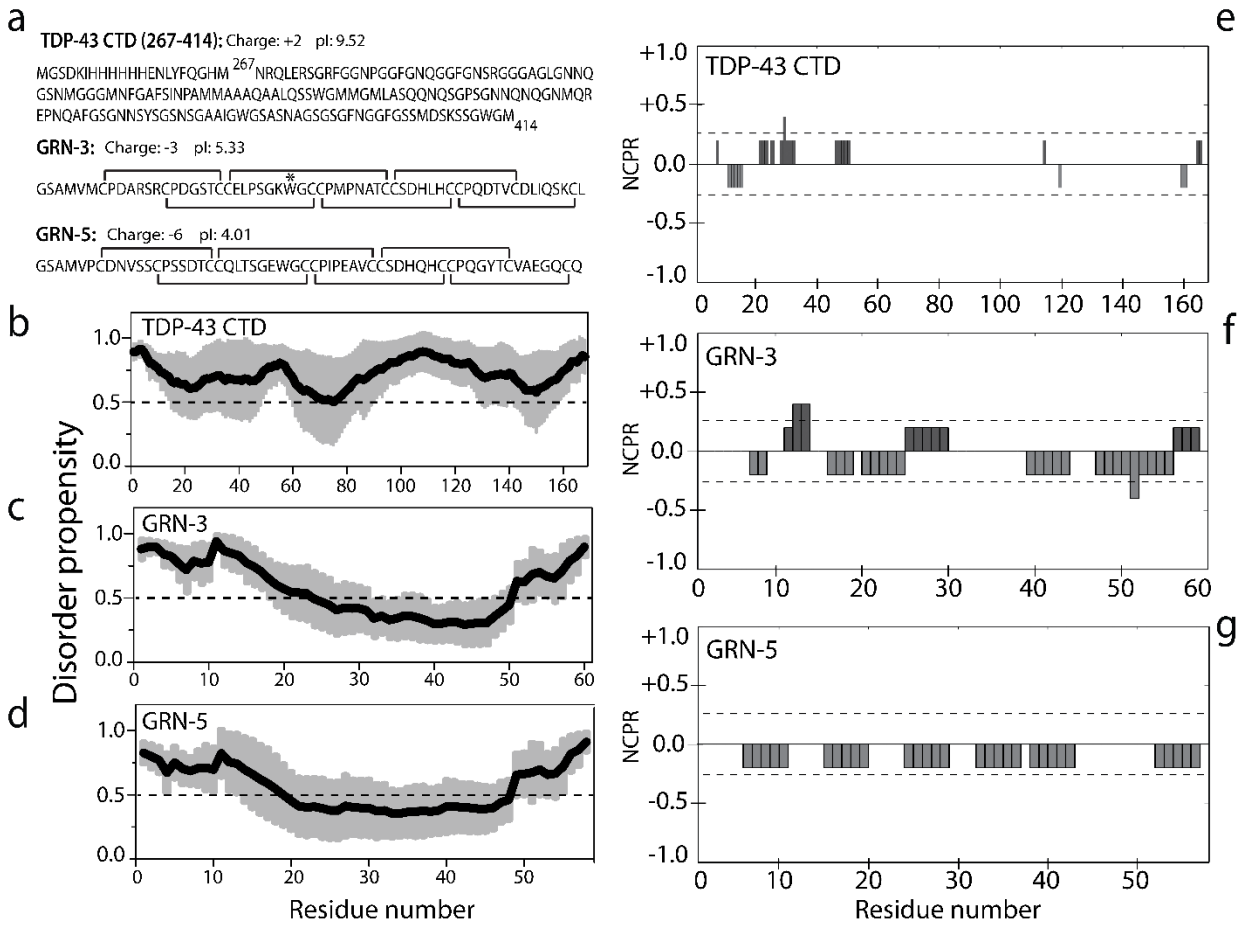

Fig 1: Sequence, disorder and charge distributions of the proteins used in this study. a) The sequence of TDP-43 C-terminal domain (TDP-43 CTD) (267-414; 14.5 kDa) which constitutes the major part of the toxic 25 kDa TDP-43 C-terminal fragment with a hexa histidine-tag on the N-terminus. Sequences of GRN-3 and GRN-5 with putative disulfide bonds. A conservative mutation of Y to W (indicated as *) was made to GRN-3, which is a conserved residue in all GRNs. Both GRNs were used in fully reduced (free thiols) and oxidized conditions in this study. Computational evaluation of the per-residue intrinsic disorder predispositions of TDP-43 CTD (b), GRN-3 (c), and GRN-5 (d). Here, the outputs of PONDR® VLXT, PONDR® FIT, PONDR® VL3, PONDR® VSL2, IUPred_S and IUPred_L were averaged to generate mean disorder profiles of different computational data query proteins. Diagrams of linear net charge per residue (NCPR) for TDP-43 CTD (e), GRN-3 (f), and GRN-5 (g) generated by CIDER computational platform (http://pappulab.wustl.edu/CIDER/).

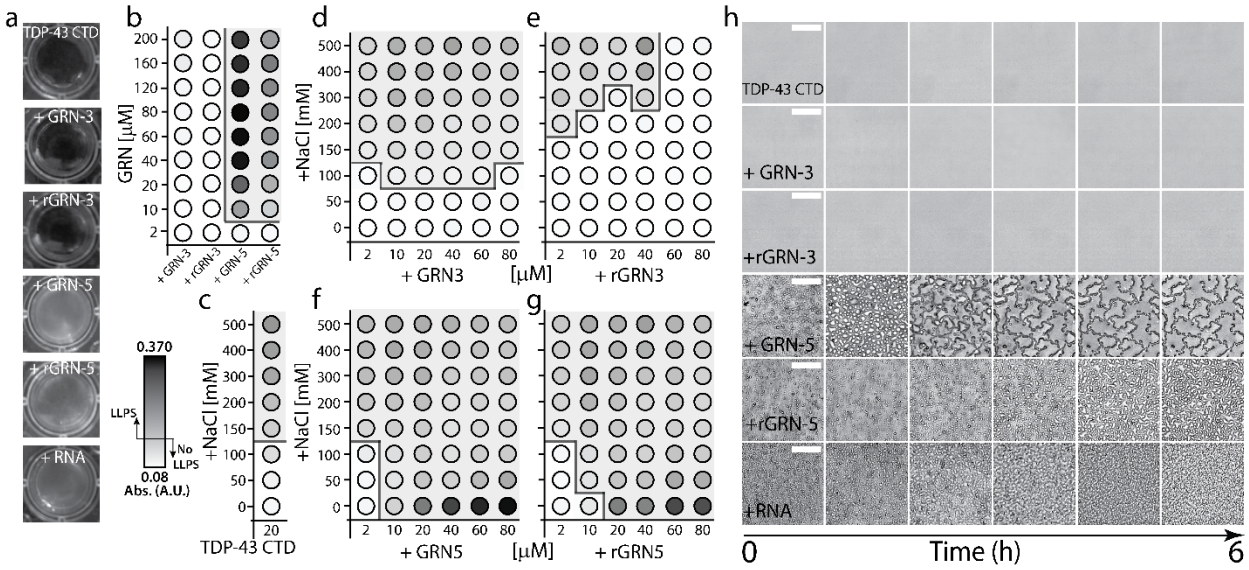

Fig 2: TDP-43 CTD undergoes LLPS in the presence of both oxidized and reduced GRN-5. a) Visual snapshots immediately after the incubations of 20 μM TDP-43 CTD in 20 mM MES buffer pH 6.0 without salt at room temperature by itself or with 40 μM GRNs in oxidized (GRN-3; GRN-5) and reduced (rGRN-3; rGRN-5) conditions along with the positive control with 40 μg/mL RNA. Only incubations with GRN-5, rGRN-5 and RNA show a turbid solution indicating phase separation. b) DIC microscopy images for the same reactions monitored for 6 hours. TDP-43 CTD by itself or with GRN-3/rGRN-3 shows the absence of liquid droplets which those with GRN-5 or rGRN-5 coalescence of the droplets to varying degrees similar to the positive control (with RNA) confirming LLPS. Scale bar represents 50 μm. c-h) Phase diagrams for TDP-43 CTD LLPS under various conditions. Phase boundary is represented by lines while grey box represents the conditions where LLPS was observed. c) LLPS of 20 μM TDP-43 CTD as a function of increasing GRN concentrations in the absence of salt. d-h) Phase diagrams for 20 μM TDP-43 CTD as a function of increasing salt and GRN concentrations for GRN-3 (e), rGRN-3 (f), GRN-5 (g) and rGRN-5 (h) along with control TDP-43 CTD in the absence of GRN (d). All phase diagrams were obtained from the turbidity of the reactions measured at 600 nm within ten minutes of incubation. The color gradient representing LLPS was generated by normalizing the absorbance values against 0-100% of black color gradient. A turbidity value of 0.11 A.U was taken as a cutoff LLPS.

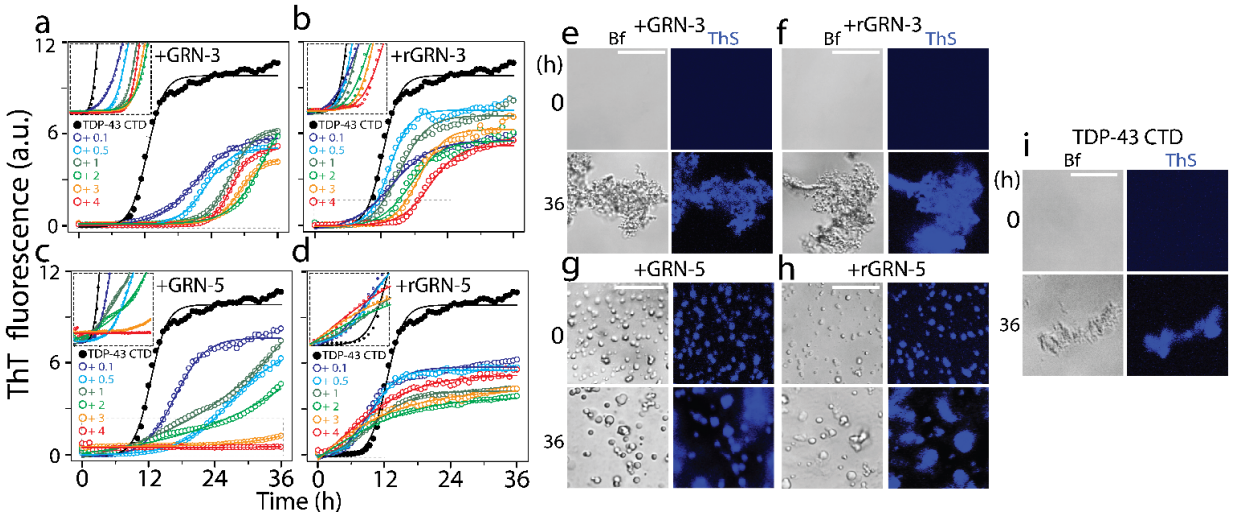

Fig 3: Modulation of TDP-43 CTD aggregation by GRNs. a-d) The aggregation kinetics of 20μM TDP-43 CTD in 20 mM MES buffer pH 6.0 at 37 °C with varying molar equivalence (2 to 80 μM) of GRN-3 (a), rGRN-3 (b), GRN-5 (c) and rGRN-5 (d), monitored by thioflavin-T (ThT) fluorescence. The inset shows the enlarged areas (boxed with dashed lines) highlighting the lag times during aggregation. The data was fitted to Boltzmann sigmoidal function. e-h) Localization of the aggregate-specific dye, thioflavin-S (ThS) observed by confocal fluorescence microscopy images on the 1:2 reaction samples of TDP-43 CTD:GRN from a-d immediately (0h) and after 36 hours of incubation. (i) Images of TDP-43 CTD control from the reaction in (a). Scale bar represents 20 μm and brightfield view is denoted by Bf.

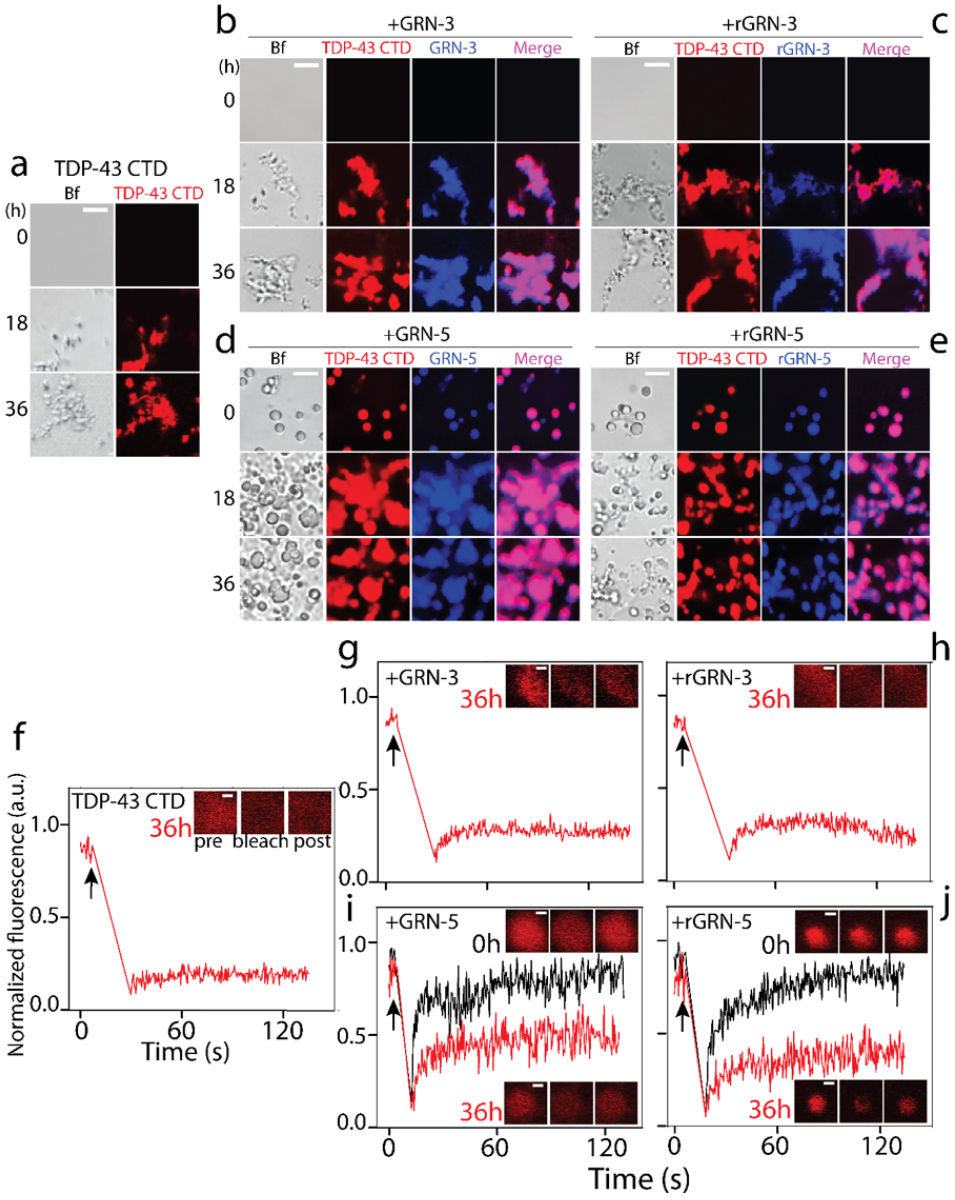

Fig 4: Coacervation of GRNs with TDP-43 CTD and dynamics of LLPS. Localization of TDP-43 CTD and GRNs was monitored on a co-incubated mixture of the two proteins in 1:2 molar ratio. A mixture containing 0.2 μM (1%) aliquot of TDP-43 CTD labeled with HiLyte 647 fluorescent tag and 20 μM unlabeled TDP-43 CTD in 20 mM MES buffer pH 6.0 at 37 °C, was co-incubated with a mixture of 40 μM GRNs containing 1% of respective proteins labeled with HiLyte 405 in separate reactions. Each of the co-incubated mixtures were visualized using DIC microscope. 'Bf' represents bright field in all the images. a) TDP-43 CTD control in the absence of GRNs shows formation of fibrillar structures after a period of 18 hours that increase in size after 36 hours. TDP-43 CTD co-incubated with GRN-3 (b) or rGRN-3 (c) show colocalization within the inclusions as well as some peripheral localization. Co-incubated samples containing GRN-5 (d) or rGRN-5 (e) show co-localization with TDP-43 CTD within droplets formed by LLPS. Scale bars in a-e represent 20 μm. f-j) Fluorescence recovery after bleaching (FRAP) performed using HiLyte 647 labeled-TDP-43 CTD. Arrow represents the time of bleaching. f) Aggregates formed

by TDP-43 CTD control show no fluorescence recovery after 36 hours. g-h) fluorescence recovery for samples containing GRN-3(g) or rGRN-3(h) immediately (0 h; black) or after 36 h of incubation (red). i-j) fluorescence recovery for samples containing GRN-5 (i) or rGRN-5 (j) immediately (0h; black) and after 36 h of incubation (red). The confocal images in the insets in f-j show the area bleached before, after, and after recovery from left to right. Scale bar represents 2 μm.

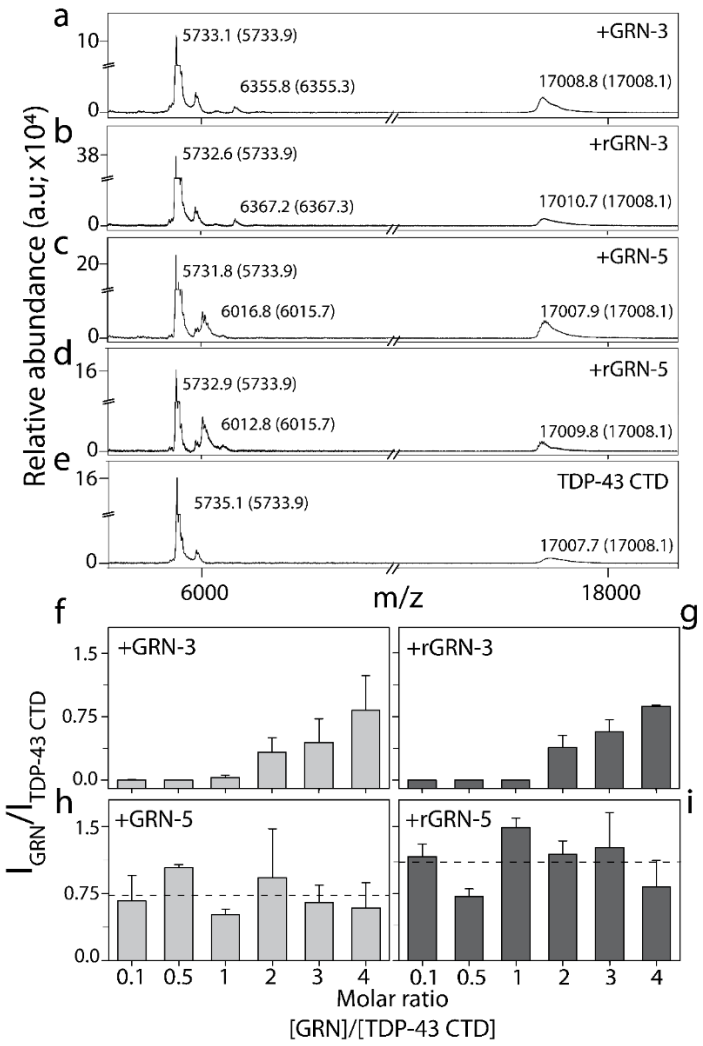

Fig 5: Quantitation of sedimented droplets and pellets from the co-incubations of TDP-43 CTD and GRNs. The co-incubated samples of TDP-43 CTD and GRNs from figures 3 and 4 were sedimented at 18,0000xg for 20 minutes after 36 hours of incubation, and the pellets were quantified by MALDI-Tof mass spectrometry using insulin (6.45 ng/μL, m.w 5733.9 Da) as an external standard. The amounts of GRN-3 (mw 6367.3 Da), GRN-5 (mw 6015.7 Da) or TDP-43 CTD (mw 17008.1 Da) within the pellets were determined with respect to the standard (detailed in Materials and Methods) and plotted as a ratio of GRN to TDP-43 CTD for the respective molar ratios. a-e) MALDI-ToF spectra of samples containing 20 uM TDP-43 CTD with 40 μM of GRN-3 (a), rGRN-3 (b), GRN-5 (c), rGRN-5 (d) and TDP-43 CTD control (e) Theoretical and observed molecular weights are shown within and outside parentheses, respectively. f-i) Ratio of intensity

of GRNs present in complex with TDP-43 CTD in samples of varying molar ratios of the former shows an increase of GRN-3 (e) and rGRN-3 (f) within the complexes at higher molar ratios, while GRN-5 (g) and rGRN-5 (h) are present in a constant amount. GRN-5 forms a 1:1 complex with TDP-43 CTD in both redox forms; GRN-5 (0.73) and rGRN-5 (1.1) as indicated by the average amount (dashed line).

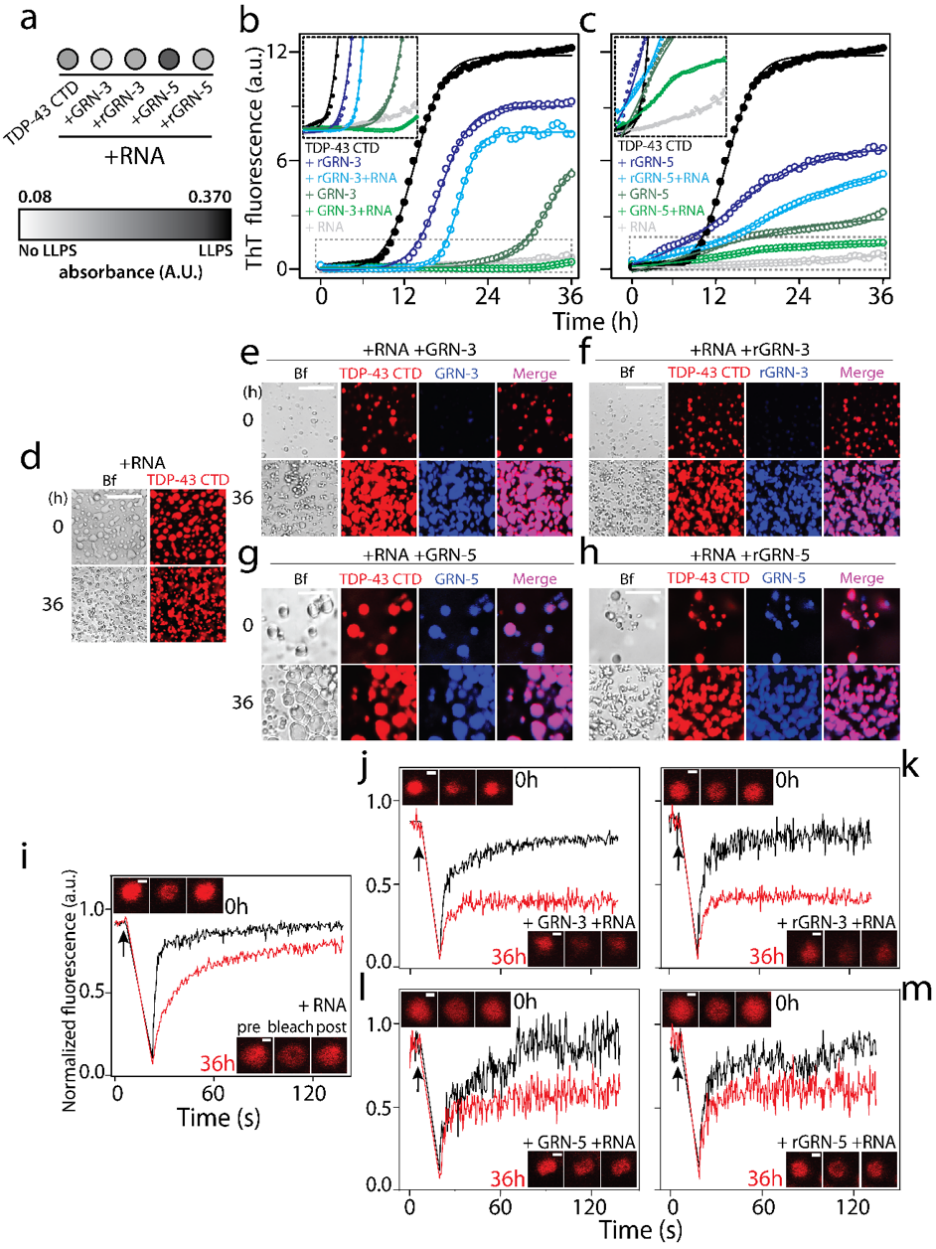

Fig 6: Modulation of TDP-43 CTD-RNA LDs by GRNs. a) Turbidity measured at 600 nm within ten minutes of incubation for the co-incubated solutions of 20 μM TDP-43 CTD with 40 μM GRN-3 or 5 (reduced and oxidized), in the presence or absence of 40 μg/mL of RNA (n=3). b-c) Aggregation kinetics of 20μM TDP-43 CTD in 20 mM MES buffer pH 6.0 at 37 °C with 40 μM of GRN-3 (b) and GRN-5 (c) in both oxidized and reduced forms, and in presence or absence of

RNA (40 µg/mL) monitored by ThT fluorescence. The inset shows the enlarged areas (boxed with dashed lines) highlighting the lag times during aggregation. d-h) Localization of the protein from the reactions similar to those in panels b and c visualized by labeling TDP-43 CTD and GRNs with HiLyte 647 and HiLyte 405, respectively (as it was done for Fig 4), and in the presence and absence of unlabeled RNA by DIC microscopy. Control sample containing TDP-43 CTD and RNA shows LDs (d). GRN-3 (e) or rGRN-3 (f) do not localize within LDs but form solid inclusions but GRN-5 (g) or rGRN-5 (h) colocalize within the LDs. Scale bars in d-h represent 20 µm. j-m) FRAP data using HiLyte 647-labeled TDP-43 CTD with LDs and GRNs immediately after incubation (0 h; black) and after 36 hours (red). Arrow represents the time of bleaching. Fluorescence recovery for samples containing control LDs(i), GRN-3(j), rGRN-3(k), GRN-5 (l) or rGRN-5 (m). The insets in i-m show confocal images of the area bleached before, after, and after the recovery from left to right. Scale bar represents 2 µm.

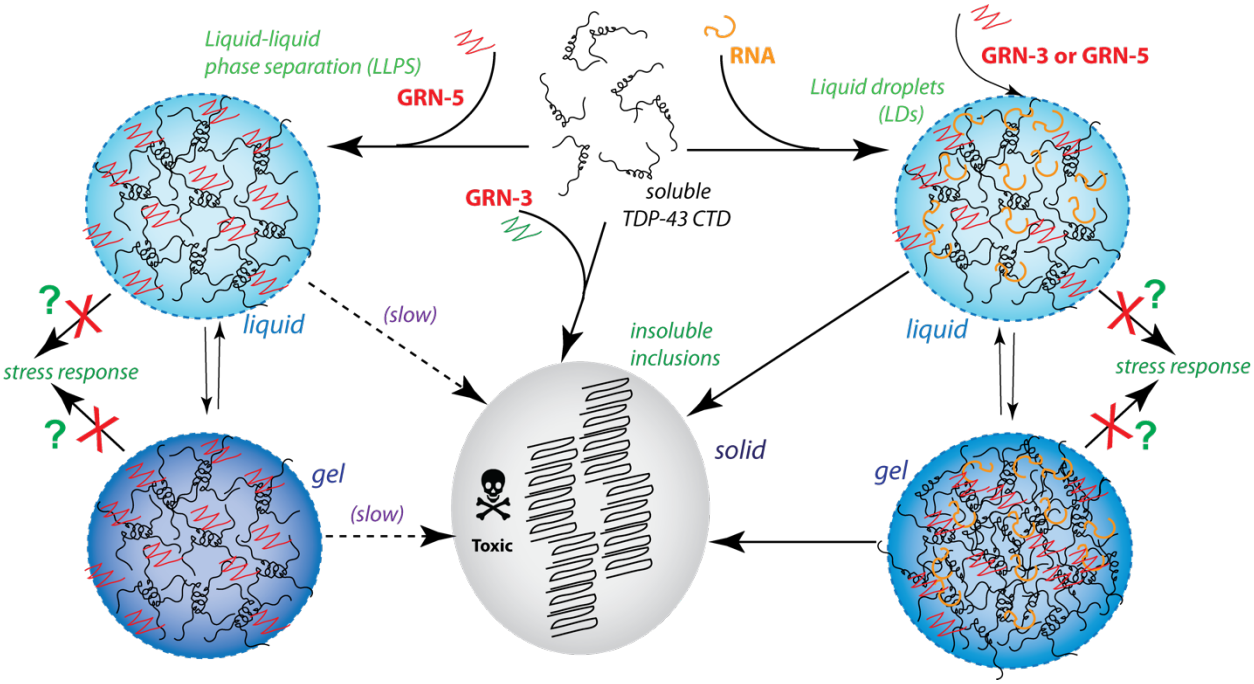

Fig 7: Schematic of the data presented in this study. GRNs selectively modulate the dynamics of TDP-43 CTD aggregation or phase separation, which may have physiological implications. The question marks indicate in this figure are possibilities unexplored in this manuscript.

Granulins modulate liquid-liquid phase separation and aggregation of prion-like C-terminal domain of the neurodegeneration-associated protein TDP-43

Anukool A Bhopatkar, Vladimir N Uversky and Vijayaraghavan Rangachari

J. Biol. Chem. published online January 6, 2020
